

DYNAMIC NUCLEAR POLARIZATION
IN SAMARIUM DOPED LANTHANUM MAGNESIUM NITRATE

by

Charles E. Byvik

Thesis submitted to the Graduate Faculty of the
Virginia Polytechnic Institute and State University
in candidacy for the degree of

DOCTOR OF PHILOSOPHY

in

Physics

September 1971

ACKNOWLEDGMENTS

I would like to thank:

Dr. David S. Wollan for suggesting this thesis topic and for sharing his enthusiasm for and his understanding of magnetic resonance;

Dr. James A. Jacobs, Dr. Thomas E. Gilmer, Dr. Ray F. Tipsword, and Dr. Clayton D. Williams for their suggestions and criticisms;

Dr. David Kaplan and Craig Ballagh for their suggestions in the treatment of the integrals, and Professor Richard A. Arndt for the use of his computer programs;

My supervisors, John P. Mugler, Jr., and Dr. L. R. Greenwood, for their patience and support, without which this work could not have been carried out;

, and for their invaluable help with the construction and repair of the many electronic components associated with the experiment;

Messrs. C. P. Moore, Jr., and his staff, M. Beasley, B. Emerson, C. Hudgins, C. D. King, J. Morris, and J. Smith, for their help in assembling the equipment needed to carry out the experiment;

for their help in preparing figures, and for typing the first draft;

The National Aeronautics and Space Administration, Langley Research Center, for providing the financial support that made this research program possible;

My parents for their encouragement and
sacrifices during the years of my formal education;

My wife and my children for
their encouragement, help, and understanding during the years needed
to complete this work.

TABLE OF CONTENTS

SECTION	PAGE
I. INTRODUCTION	1
II. THEORY	3
A. Basic Assumptions	3
B. Derivation of the Equation of Motion for the Electron Zeeman Inverse Spin Temperature, $\alpha(t)$	16
C. Derivation of the Equation of Motion for the Nuclear Zeeman Inverse Spin Temperature, $\beta(t)$	27
D. Derivation of the Equation of Motion for the Electron Dipole-Dipole Inverse Temperature, $\gamma(t)$	31
E. Effects of the Lattice Reservoir	32
F. Nuclear Spin Diffusion	34
G. Theoretical Dynamic Nuclear Polarization Results	41
III. EXPERIMENTAL APPARATUS AND PROCEDURE	43
A. Nuclear Magnetic Resonance Spectrometer	43
B. Electron Spin Resonance Spectrometer	43
C. Magnet	47
D. Cryogenic System	47
E. Sample Preparation	50
F. Experimental Procedure	51

SECTION	PAGE
IV. EXPERIMENTAL RESULTS	53
V. DISCUSSION OF RESULTS AND CONCLUSIONS	66
VI. BIBLIOGRAPHY	72
VII. APPENDIX	
A. Complete Expression of the Steady-State Enhancement	74
VIII. VITA	76

LIST OF FIGURES AND TABLES

FIGURE	PAGE
1. Apparatus used in the DNP experiments	44
2. Block diagram of the nuclear magnetic resonance spectrometer	45
3. Block diagram of the electron spin resonance spectrometer	46
4. Sketch of the cryogenic sample probe	48
5. Schematic of the cryogenic system	49
6. The derivative of the ESR absorption line for crystal 4	57
7. Enhancement curve for crystal 2 at 3.06° K	58
8. Enhancement of the polarization peak as a function of relative microwave power for crystal 2	59
9. Enhancement curve for crystal 6 at 3.0° K	60
10. Enhancement of the polarization peak as a function of relative microwave power for crystal 6	61
11. The inverse of the nuclear spin-lattice relaxation time of crystal 7 versus bath temperature for $H = 8970$ Oe	63
12. Theoretical enhancement curve assuming a Gaussian line shape for the ESR and the experimental data for crystal 4	65

TABLE	PAGE
I. Summary of Experimental Parameters	54
II. Nuclear Relaxation and Spin Diffusion Parameters for Sm:LMN	70

I. INTRODUCTION

In 1953, Overhauser^{1,2} proposed that the polarization of nuclei in a metallic solid could be changed from its thermal equilibrium value through the contact hyperfine interaction of the nuclei with the conduction electrons by saturating the electron spin resonance transition. The idea of dynamic polarization of nuclei was soon extended to non-metallic materials.³⁻⁶ Experimental verification of dynamic nuclear polarization in metals was reported in 1956.⁷

Dynamic nuclear polarization (DNP) in ionic solids can occur if paramagnetic nuclei interact with nearby paramagnetic atoms through the magnetic dipole-dipole interaction. This is called DNP by the "solid effect" and is the subject of this thesis. Two approaches have been used to describe the dynamics of the "solid effect": the rate equation approach of Jeffries and co-workers⁸⁻¹¹ and of Borghini,¹² and the spin temperature theory.¹³⁻¹⁷ The rate equation approach assumes that the "solid effect" may be described completely by following the time evolution of the populations of the electronic and nuclear Zeeman levels. This approach can lead to erroneous results if the spins are strongly interacting. The spin temperature theory includes the effect of the strong spin-spin coupling as well as the Zeeman interactions and the lattice in a relatively simple way. Within certain limits, to be discussed later, the Zeeman and the spin-spin interactions and the lattice can each be assigned a thermodynamic reservoir having a temperature and specific heat. The reservoirs exchange energy with each other through

the applied radio frequency fields, certain dipolar interactions and spin-lattice interactions. The expression for the steady state nuclear polarization resulting from the spin temperature approach reduces to the expression obtained by the rate equation of the Zeeman populations (except for a small correction term) in the limit where the electronic resonance linewidth is smaller than the nuclear resonance frequency. A material exhibiting this limit is diamagnetic lanthanum magnesium nitrate in which a small percentage of the lanthanum ions are replaced by paramagnetic samarium ions. At about 9 kOe, 9.2 GHz, and liquid helium temperatures, the electron spin resonance linewidth of samarium in this crystal is of the order of 5 MHz¹⁸ and the nuclear resonance frequency of the protons in the waters of hydration is 38 MHz. This thesis will compare the results of measurements of the dynamic polarization of protons in a number of single crystals of samarium ions in lanthanum magnesium nitrate (Sm:LMN) with the results of the spin temperature theory of the "solid effect."

II. THEORY

A. Basic Assumptions

A derivation of the equations governing the DNP by the "solid effect" will be made in this section. The density matrix and spin temperature theory will be the approach used in this derivation as opposed to the rate equation approach.⁸⁻¹² The spin temperature theory has the advantage that the effects of the dipole-dipole interactions may be included, and yields analytical expressions for the lineshapes. A detailed derivation of the "solid effect" using spin temperature theory is felt necessary as (1) it is not available in the literature, (2) the published equations governing the "solid effect" are either incomplete or contain sign errors, and (3) all of the assumptions made are not clearly stated. (Note in particular ref. 13-17.)

Consider a solid containing N paramagnetic ions per unit volume (which will henceforth be called "electrons") having an effective spin $S = 1/2$ and n nuclei per unit volume having a spin $I = 1/2$. The effective Hamiltonian for this paramagnetic system when placed in a homogeneous magnetic field which has a steady component \vec{H}_0 and a high frequency component $\vec{H}_1(t)$ is given as¹⁹

$$\mathcal{H} = \mathcal{H}_{SZ} + \mathcal{H}_{IZ} + \mathcal{H}_{SS} + \mathcal{H}_{II} + \mathcal{H}_{IS} + \mathcal{H}_{SL} + \mathcal{H}_{IL} + \mathcal{H}_{rf} \quad (1)$$

where the terms are the electron Zeeman, the nuclear Zeeman, the electron dipole-dipole, the nuclear dipole-dipole, the electron-nuclear dipole-dipole, the electron spin-lattice, the nuclear spin-lattice and

the radio frequency interaction Hamiltonians. Explicitly, they are

$$\mathcal{H}_{\text{SZ}} = \gamma_e \hbar \sum_{j=1}^N \vec{S}_j \cdot \vec{H}_0 \quad (2)$$

$$\mathcal{H}_{\text{IZ}} = \gamma_n \hbar \sum_{l=1}^n \vec{I}_l \cdot \vec{H}_0 \quad (3)$$

$$\mathcal{H}_{\text{SS}} = \gamma_e^2 \hbar^2 \sum_{i>j=1}^N r_{ij}^{-3} \left[\vec{S}_i \cdot \vec{S}_j - 3r_{ij}^{-2} (\vec{S}_i \cdot \vec{r}_{ij})(\vec{S}_j \cdot \vec{r}_{ij}) \right] \quad (4)$$

$$\mathcal{H}_{\text{II}} = \gamma_n^2 \hbar^2 \sum_{k>l=1}^n R_{kl}^{-3} \left[\vec{I}_k \cdot \vec{I}_l - 3R_{kl}^{-2} (\vec{I}_k \cdot \vec{R}_{kl})(\vec{I}_l \cdot \vec{R}_{kl}) \right] \quad (5)$$

$$\mathcal{H}_{\text{IS}} = \gamma_e \gamma_n \hbar^2 \sum_{k=1}^N \sum_{l=1}^n d_{kl}^{-3} \left[\vec{S}_k \cdot \vec{I}_l - 3d_{kl}^{-2} (\vec{S}_k \cdot \vec{d}_{kl})(\vec{I}_l \cdot \vec{d}_{kl}) \right] \quad (6)$$

$$\mathcal{H}_{\text{rf}} = \gamma_e \hbar \sum_{k=1}^N \vec{H}_1(t) \cdot \vec{S}_k + \gamma_n \hbar \sum_{l=1}^n \vec{H}_1(t) \cdot \vec{I}_l \quad (7)$$

where γ_n (γ_e) is the nuclear (electron) gyromagnetic ratio, both assumed to be inherently negative; \hbar is Planck's constant divided by 2π ; \vec{r}_{ij} is the vector distance between the S_i -th and S_j -th electron; \vec{R}_{kl} is the vector distance between the I_k -th and I_l -th nuclear spin; \vec{d}_{kl} is the vector distance between the S_k -th electron and the I_l -th

nuclear spin; and \vec{H}_1 is the high frequency magnetic field interacting with the electrons and nuclei. The \mathcal{H}_{SL} and \mathcal{H}_{IL} terms are discussed by Jeffries.⁸

The following assumptions are now introduced.

1. The magnetic field H_0 is much larger than the magnetic field experienced by each dipole due to the neighboring dipoles. The latter field is called the local magnetic field.

2. The magnitude of the electron gyromagnetic ratio γ_e is much larger than that of the nuclear gyromagnetic ratio, γ_n .

3. The electron and nuclear spin-lattice relaxation times, T_e and T_n , are very long compared to the electron and nuclear spin-spin relaxation times, T_{2e} and T_{2n} , respectively, and there exists times t such that

$$T_{2e}, T_{2n} \ll t \ll T_e, T_n, W_0^{-1}, \left(\frac{n}{N} W_1\right)^{-1}, \left(\frac{n}{N} W^\pm\right)^{-1}, \quad (8)$$

where the terms $W_0^{-1}, \left(\frac{n}{N} W_1\right)^{-1}, \left(\frac{n}{N} W^\pm\right)^{-1}$ will be discussed later.

4. The effects of the lattice may be ignored for times τ satisfying the inequality (8) and the rate of energy exchange between the various spin systems and the high frequency magnetic field $\vec{H}_1(t)$ calculated. The effect of the lattice is then reintroduced.

5. The electron and nuclear resonance lines are homogeneously broadened.²⁰

Consider the large constant magnetic field \vec{H}_0 to be applied along the z-axis in the laboratory reference frame. Then

$$\mathcal{H}_{SZ} = \gamma_e \hbar H_0 \sum_{j=1}^N S_{zj} \quad (9)$$

and

$$\mathcal{H}_{IZ} = \gamma_n \hbar H_0 \sum_{l=1}^n I_{zl} \quad (10)$$

Define

$$\omega_e = \gamma_e H_0 \quad (11)$$

$$\omega_n = \gamma_n H_0 \quad (12)$$

$$S_z = \sum_{j=1}^N S_{zj} \quad (13)$$

$$I_z = \sum_{l=1}^n I_{zl} \quad (14)$$

where ω_e and ω_n are the electron and nuclear Larmor frequencies, and S_z and I_z are the z-components of the total spin of S- and I-spins, respectively. Since $\gamma_e \gg \gamma_n$, one has $\omega_e \gg \omega_n$; thus if an oscillating field $\vec{H}_1(t)$ of frequency ω is of the order ω_e , then the direct interaction of the nuclear spins with this field is negligible. We apply this oscillating field in a plane perpendicular to \vec{H}_0 , so that equation (7) becomes

$$\mathcal{H}_{\text{rf}} = \gamma_e \hbar H_1 \sum_{k=1}^N (S_{xk} \cos \omega t + S_{yk} \sin \omega t)$$

or

$$\mathcal{H}_{\text{rf}} = \gamma_e \hbar H_1 (S_x \cos \omega t + S_y \sin \omega t),$$

where S_x and S_y are defined in a fashion similar to S_z in equation (13). Defining $\omega_1 = \gamma_e H_1$ and noting the identity

$$e^{-i\omega S_z t} S_x e^{+i\omega S_z t} = S_x \cos \omega t + S_y \sin \omega t,$$

then

$$\mathcal{H}_{\text{rf}} = \hbar \omega_1 e^{-i\omega S_z t} S_x e^{+i\omega S_z t}. \quad (15)$$

It is convenient to write the various dipolar interactions as

$$\mathcal{H}_{\text{SS}} = \gamma_e^2 \hbar^2 \sum_{k>l=1}^N r_{kl}^{-3} \left\{ A_{kl} + B_{kl} + C_{kl} + D_{kl} + E_{kl} + F_{kl} \right\} \quad (16a)$$

where

$$\begin{aligned} A_{kl} &= S_{zk} S_{zl} (1 - 3 \cos^2 \theta_{kl}) \\ B_{kl} &= -\frac{1}{4} (1 - 3 \cos^2 \theta_{kl}) (S_k^+ S_l^- + S_k^- S_l^+) \\ C_{kl} &= -\frac{3}{2} \sin \theta_{kl} \cos \theta_{kl} e^{-i\varphi_{kl}} (S_{zk} S_l^+ + S_{zl} S_k^+) \\ D_{kl} &= -\frac{3}{2} \sin \theta_{kl} \cos \theta_{kl} e^{i\varphi_{kl}} (S_{zk} S_l^- + S_{zl} S_k^-) \end{aligned} \quad (16b)$$

$$\begin{aligned}
E_{kl} &= -\frac{3}{4} \sin^2 \theta_{kl} e^{-2i\varphi_{kl}} S_k^+ S_l^+ \\
F_{kl} &= -\frac{3}{4} \sin^2 \theta_{kl} e^{+2i\varphi_{kl}} S_k^- S_l^-,
\end{aligned} \tag{16b}$$

where θ_{kl} and φ_{kl} are the polar coordinates of the vector \vec{r}_{kl} , the z-axis is parallel to \vec{H}_0 , and

$$S_k^\pm = S_{xk} \pm i S_{ky}.$$

\mathcal{H}_{IS} and \mathcal{H}_{II} can be similarly written. The effective Hamiltonian now has the form

$$\mathcal{H}' = \omega_e S_z + \omega_n I_z + \mathcal{H}_{SS} + \mathcal{H}_{IS} + \mathcal{H}_{II} + \omega_1 e^{-i\omega S_z t} S_x e^{i\omega S_z t} \tag{17}$$

where the prime indicates that the spin-lattice interactions have been omitted. Note that the Hamiltonian has been written in frequency units, i.e., $\hbar = 1$.

The time evolution of the system described by the Hamiltonian can be determined from the equation of motion of the density matrix, ρ , for the system. The density matrix obeys the relation²¹

$$\frac{d\rho}{dt} = i[\rho, \mathcal{H}'], \tag{18}$$

again taking $\hbar = 1$.

Following Redfield,²² we transform the density matrix by a unitary transformation, $R(t)$, to a frame of reference rotating about the

laboratory z-axis at a frequency ω . Thus

$$\rho^R(t) = R(t) \rho(t) R^{-1}(t) ,$$

where $\rho^R(t)$ is the density matrix in the rotating frame and

$$R(t) = e^{i\omega S_z t} . \quad (20)$$

We do not transform the nuclear spins because they are not subject to saturating rf fields in these experiments. See Wollan²³ for a discussion of this point.

The equation of motion for the density matrix then becomes

$$\frac{d\rho^R}{dt} = i[\rho^R(t), \mathcal{H}^R(t)] \quad (21)$$

where

$$\mathcal{H}^R(t) = \Delta S_z + \omega_n I_z + \omega_1 S_x + R(t) \left\{ \mathcal{H}_{SS} + \mathcal{H}_{IS} + \mathcal{H}_{II} \right\} R^{-1}(t) \quad (22)$$

and

$$\Delta = \omega_e - \omega . \quad (23)$$

\mathcal{H}_{II} is not altered by the unitary transformation since

$$\left[R(t), \mathcal{H}_{II} \right] = 0 .$$

\mathcal{H}_{SS} and \mathcal{H}_{IS} are of the form

$$R(t) \mathcal{H}_{SS} R^{-1}(t) = \mathcal{H}_{SS}^{\circ} + \sum_m \mathcal{H}_{SS}^m$$

$$R(t) \mathcal{H}_{IS} R^{-1}(t) = \mathcal{H}_{IS}^{\circ} + \sum_m \mathcal{H}_{IS}^m \quad (24)$$

where the sums are over the values $m = \pm 1, \pm 2$. \mathcal{H}_{SS}° and \mathcal{H}_{IS}° are the secular parts of the dipolar Hamiltonians, i.e., those which commute with $R(t)$:

$$\left[\mathcal{H}_{IS}^{\circ}, R(t) \right] = \left[\mathcal{H}_{SS}^{\circ}, R(t) \right] = 0, \quad (25)$$

and \mathcal{H}_{SS}^m and \mathcal{H}_{IS}^m are the nonsecular parts of the dipolar interactions. The nonsecular terms in equation (24) oscillate at frequencies $\pm\omega, \pm 2\omega$ in the rotating reference frame and may be ignored as discussed by Redfield²² and Goldman.¹⁶ Then from equations (16) and (25)

$$\mathcal{H}_{SS}^{\circ} = \gamma_e^2 \sum_{k>l=1}^N r_{kl}^{-3} \left\{ A_{kl} + B_{kl} \right\} \quad (26)$$

and

$$\mathcal{H}_{IS}^{\circ} = \sum_{k=1}^N \sum_{l=1}^n \left\{ \epsilon_{kl}^{\circ} S_{zk} I_{zl} + \epsilon_{kl} S_{zk} I_{zl}^+ + \epsilon_{kl}^* S_{zk} I_{zl}^- \right\} \quad (27)$$

where

$$\epsilon_{kl}^{\circ} = \gamma_e \gamma_n d_{kl}^{-3} (1 - 3 \cos^2 \theta_{kl}) \quad (28)$$

$$\epsilon_{kl} = -\frac{3}{2} \gamma_e \gamma_n \sin \theta_{kl} \cos \theta_{kl} e^{-i\phi_{kl}} d_{kl}^{-3} \quad (29)$$

and the star indicates complex conjugate. The Hamiltonian in the rotating frame is reduced to

$$\mathcal{H}^R = \Delta S_z + \omega_n I_z + \omega_1 S_x + \mathcal{H}_{SS}^{\circ} + \mathcal{H}_{IS}^{\circ} + \mathcal{H}_{II} . \quad (30)$$

We define

$$\mathcal{H}_0 = \Delta S_z + \omega_n I_z + \mathcal{H}_{SS}^{\circ} \quad (31)$$

and

$$V = \omega_1 S_x + \mathcal{H}_{IS}^{\circ} + \mathcal{H}_{II} . \quad (32)$$

Then

$$\mathcal{H}^R = \mathcal{H}_0 + V . \quad (33)$$

Transforming to the interaction representation by a unitary transformation

$$\rho^I(t) = U^{-1}(t) \rho^R(t) U(t) \quad (34)$$

where

$$U(t) = e^{-i\mathcal{H}_0 t} , \quad (35)$$

one has

$$\frac{d\rho^I}{dt} = i \left[\rho^I, V^I(t) \right] \quad (36)$$

where

$$V^I(t) = U^{-1}(t)V U(t) . \quad (37)$$

Equation (36) may be integrated and then iterated to obtain the form

$$\begin{aligned} \rho^I(t) = & \rho^I(0) + \sum_{n=1}^{\infty} (i)^n \int_0^t dt_1 \int_0^{t_1} dt_2 \dots \int_0^{t_{n-1}} dt_n \\ & \times \left[\left[\dots \left[\rho^I(0), V^I(t_n) \right], V^I(t_{n-1}) \right], \dots \right], V^I(t_1) \right], \quad (38) \end{aligned}$$

and this result differentiated to obtain

$$\begin{aligned} \frac{d\rho^I}{dt} = & i \left[\rho^I(0), V^I(t) \right] + \sum_{n=1}^{\infty} (i)^{n+1} \int_0^t dt_1 \int_0^{t_1} dt_2 \dots \int_0^{t_{n-1}} dt_n \\ & \times \left[\left[\dots \left[\rho^I(0), V^I(t_n) \right], V^I(t_{n-1}) \right], \dots \right], V^I(t) \right]. \quad (39) \end{aligned}$$

Note that $\rho^I(0) = \rho^R$.

The basis of the spin temperature theory is to assume at this point that the density matrix in the rotating frame will have the canonical form for times t satisfying equation (8). The justification for this assumption is discussed in references 16, 22, and 24. For this system, it is assumed that the commuting terms ΔS_z , $\alpha_n I_z$, and \mathcal{H}_{SS}^0 can be considered as thermodynamic reservoirs having inverse temperatures α , β , and γ , respectively. Each reservoir is considered to reach internal equilibrium in a time of the order of its spin-spin relaxation time.

Therefore, we assume that

$$\rho^R(t) = \frac{e^{-\alpha(t)\Delta S_z - \beta(t)\omega_n I_z - \gamma(t)\mathcal{H}_{SS}^0}}{\text{Tr } e^{-\alpha(t)\Delta S_z - \beta(t)\omega_n I_z - \gamma(t)\mathcal{H}_{SS}^0}}. \quad (40)$$

The inverse temperature, α , is defined as

$$\alpha = \frac{1}{kT_{ez}}$$

where k is the Boltzmann constant and T_{ez} is the electron Zeeman spin temperature. The inverse temperatures β and γ are similarly defined.

The electron-nuclear dipole-dipole reservoir and the nuclear dipole-dipole reservoir have been ignored in equation (40) as well as the off-diagonal part of the density matrix. The electron-nuclear dipole-dipole reservoir (i.e., the $S_{zk}I_{zl}$ terms in equation (27)) contributes to the inhomogeneous broadening of the resonance lines and is assumed to be negligible.²⁰ This term will also give rise to a barrier to spin diffusion and this will be treated phenomenologically when spin diffusion is taken into account in section II F. The off-diagonal $S_{zk}I_l^{\pm}$ terms in \mathcal{H}_{IS}^0 are retained in V as a perturbation. The nuclear dipole-dipole interaction may be ignored since its frequency (~ 50 kHz) is very small compared to those of the electron Zeeman, nuclear Zeeman, and electron dipole-dipole interactions in the rotating frame (all ~ 5 MHz). This term will be important only when spin

diffusion is taken into account. The size of the contribution made by the off-diagonal part of the density matrix is discussed by Goldman¹⁶ and for the time scale considered here, the off-diagonal part may be ignored. With these approximations, we note that

$$\rho^I(t) = \rho^R(t) .$$

The representation used for the electron system is one in which \mathcal{H}_{SS}^0 and S_z are diagonal. Since the nuclear dipole-dipole interaction has been neglected, the nuclei are considered independent particles and the representation used is one in which all the single particle operators I_l^2 and I_{zl} are diagonal.

In the high temperature approximation, one has

$$\rho^R(t) = \eta^{-1} \left\{ 1 - \alpha(t)\Delta S_z - \beta(t) \omega_n I_z - \gamma(t) \mathcal{H}_{SS}^0 \right\} , \quad (41)$$

where η is the normalizing factor. This approximation is necessary to make the calculation tractable, and corresponds to the experimental conditions encountered in this work.

Note that the electron and nuclear magnetizations along the z-axis are proportional to the ensemble average of the operators S_z and I_z , respectively. Using the density matrix, these values are found as

$$\langle S_z \rangle = \text{Tr} \rho^R(t) S_z$$

and

$$\langle I_z \rangle = \text{Tr} \rho^R(t) I_z$$

where $\langle \rangle$ indicates the canonical ensemble average value and Tr indicates a sum over the diagonal elements in a space that includes both the electron and nuclear eigenstates. It follows that the time rate of change of these expectation values are (in the high temperature limit)

$$\frac{d\langle S_z \rangle}{dt} = \text{Tr} \frac{d\rho^R(t)}{dt} S_z = -\Delta\eta^{-1} \text{Tr} S_z^2 \frac{d\alpha}{dt} \quad (42)$$

and

$$\frac{d\langle I_z \rangle}{dt} = \text{Tr} \frac{d\rho^R(t)}{dt} I_z = -\omega_n \eta^{-1} \text{Tr} I_z^2 \frac{d\beta}{dt} \quad (43)$$

It can be noted from (42) and (43) that the changes in the magnetization are proportional to the changes of the corresponding inverse temperatures of the reservoirs. The calculation of the time evolution of the inverse temperatures using equations (39), (41), (42), and (43) follows.

B. Derivation of the Equation of Motion for the
Electron Zeeman Inverse Spin
Temperature, $\alpha(t)$

From equations (39) and (42),

$$\begin{aligned}
-(\Delta \text{Tr} S_z^2) \frac{d\alpha}{dt} = & i \eta \text{Tr} [\rho^R, v(t)] S_z + (i)^2 \eta \text{Tr} \int_0^t dt' \left[[\rho^R, v(t')], v(t) \right] S_z \\
& + (i)^3 \eta \text{Tr} \int_0^t dt' \int_0^{t'} dt'' \left[\left[[\rho^R, v(t'')], v(t') \right], v(t) \right] S_z \\
& + (i)^4 \eta \text{Tr} \int_0^t dt' \int_0^{t'} dt'' \int_0^{t''} dt''' \\
& \times \left[\left[\left[[\rho^R, v(t''')], v(t'') \right], v(t') \right], v(t) \right] S_z + \dots \quad (44)
\end{aligned}$$

where the superscript I, indicating the interaction representation, has been dropped. Assuming the trace and the time integrals commute, the following terms must be evaluated:

$$\begin{aligned}
C_1 & \equiv \eta \text{Tr} [\rho^R, v(t)] S_z \\
C_2 & \equiv \eta \text{Tr} \left[[\rho^R, v(t')], v(t) \right] S_z \\
C_3 & \equiv \eta \text{Tr} \left[\left[[\rho^R, v(t'')], v(t') \right], v(t) \right] S_z \\
C_4 & \equiv \eta \text{Tr} \left[\left[\left[[\rho^R, v(t''')], v(t'') \right], v(t') \right], v(t) \right] S_z . \quad (45)
\end{aligned}$$

Using the identity

$$\text{Tr} [A, B] C = \text{Tr} A [B, C] , \quad (46)$$

one has

$$C_1 = \eta \text{Tr} [S_z, \rho^R] V(t) = 0 , \quad (47)$$

since

$$[S_z, \rho^R] = 0 .$$

Using the same identity

$$C_2 = \eta \text{Tr} \left\{ [\rho^R, V(t')] \right\} \left\{ [V(t), S_z] \right\} . \quad (48)$$

$\rho^R(t)$ can be written in the following way

$$\rho^R = \eta^{-1} \left\{ 1 - (\alpha - \gamma) S_z - (\beta - \gamma) \omega_n I_z - \gamma \mathcal{H}_0 \right\} . \quad (49)$$

Recalling that

$$V(t) = \omega_1 S_x(t) + \mathcal{H}_{IS}^0(t) ,$$

where $S_{x,y}(t)$ and $\mathcal{H}_{IS}^0(t)$ are in the interaction representation, we have

$$\begin{aligned} C_2 &= -\omega_1^2 \Delta(\alpha - \gamma) \text{Tr} S_y(t') S_y(t) \\ &\quad + i \omega_1 \omega_n (\beta - \gamma) \text{Tr} S_y(t) [I_z, \mathcal{H}_{IS}^0(t')] \\ &\quad + i \gamma \omega_1 \text{Tr} S_y(t) [\mathcal{H}_0, V(t')] . \end{aligned} \quad (50)$$

The second term is zero as can easily be seen using equation (46) and noting that

$$[S_y(t), I_z] = 0 .$$

Using

$$i \operatorname{Tr} S_y(t) [\mathcal{H}_0, V(t)] = \frac{d}{dt'} \operatorname{Tr} S_y(t - t') V ,$$

and integrating C_2 as noted in (44), we get

$$\begin{aligned} \int_0^t dt' C_2 &= -\omega_1^2 \Delta(\alpha - \gamma) \int_0^t dt' \operatorname{Tr} S_y S_y(t - t') \\ &+ \gamma \omega_1 \int_0^t dt' \frac{d}{dt'} \operatorname{Tr} S_y(t - t') V . \end{aligned} \quad (51)$$

The second term in (51) is also zero. This is shown by letting $\tau = t - t'$; then

$$\int_0^t dt' \frac{d}{dt'} \operatorname{Tr} [S_y(t - t') V] = - \int_0^t d\tau \left\{ \frac{d}{d\tau} \operatorname{Tr} [\omega_1 S_x S_y(\tau) + S_y(\tau) \mathcal{H}_{IS}^0] \right\} . \quad (52)$$

But

$$\operatorname{Tr} S_y(\tau) \mathcal{H}_{IS}^0 = \operatorname{Tr} S_y(\tau) \left[\sum_{k=1}^N \sum_{l=1}^n (\epsilon_{kl} S_{zk} I_l^+ + \epsilon_{kl}^* S_{zk} I_l^-) \right] = 0 \quad (53)$$

since I_l^\pm has no diagonal elements. Noting the identity

$$S_y(\tau) = -\tilde{S}_x(\tau) \sin \Delta\tau + \tilde{S}_y(\tau) \cos \Delta\tau, \quad (54)$$

where

$$\tilde{S}_{x,y}(\tau) = e^{i\mathcal{H}_{SS}^0 \tau} S_{x,y} e^{-i\mathcal{H}_{SS}^0 \tau}, \quad (55)$$

the remaining term in (51) becomes

$$\begin{aligned} -\omega_1 \int_0^t d\tau \frac{d}{d\tau} [\text{Tr} S_x S_y(\tau)] &= \\ = -\omega_1 \int_0^t d\tau \frac{d}{d\tau} [\text{Tr} S_x \tilde{S}_y(\tau) \cos \Delta\tau - \text{Tr} S_x \tilde{S}_x(\tau) \sin \Delta\tau]. \end{aligned}$$

Note that

$$\text{Tr} S_x \tilde{S}_y(\tau) = 0,$$

since a rotation of π about the y-axis sends S_x into $-S_x$ and leaves $\tilde{S}_y(\tau)$ unchanged. Since the trace is invariant the result follows. Then

$$-\omega_1 \int_0^t d\tau \frac{d}{d\tau} [\text{Tr} S_x S_y(\tau)] = \omega_1 \int_0^t d\tau \frac{d}{d\tau} \text{Tr} S_x \tilde{S}_x(\tau) \sin \Delta\tau.$$

The term $\text{Tr} S_x \tilde{S}_x(\tau)$ is proportional to the correlation function of the transverse magnetization, with a correlation time $\sim T_{2e}$. Since t is assumed to be very much larger than T_{2e} , the upper limit of the integration may be taken to infinity. Thus

$$-\omega_1 \int_0^\infty d\tau \frac{d}{d\tau} [\text{Tr} S_x S_y(\tau)] = \omega_1 [\text{Tr} S_x \tilde{S}_x(\tau) \sin \Delta\tau] \Big|_{\tau=0}^{\tau=\infty} = 0,$$

since the correlation function is zero at $\tau = \infty$. Equation (51) is reduced to

$$\int_0^t dt' c_2 = -\omega_1^2 \Delta(\alpha - \gamma) \int_0^\infty dt' \text{Tr} S_y S_y(t - t').$$

Using exactly the same arguments as used above

$$\int_0^t dt' c_2 = -\omega_1^2 \Delta(\alpha - \gamma) \int_0^\infty d\tau \text{Tr} S_y \tilde{S}_y(\tau) \cos \Delta\tau. \quad (56)$$

c_3 may be calculated using some of the relations developed in finding c_2 . Expanding c_3 we get

$$\begin{aligned} c_3 &= -\omega_1^2 \Delta(\alpha - \gamma) \text{Tr} S_y(t'') [\mathcal{H}_{IS}^0(t'), S_y(t)] \\ &\quad + i\omega_n \omega_1^2 (\beta - \gamma) \text{Tr} [I_z, \mathcal{H}_{IS}^0(t'')] [S_x(t'), S_y(t)] \\ &\quad + i\omega_1 \omega_n (\beta - \gamma) \text{Tr} [I_z, \mathcal{H}_{IS}^0(t'')] [\mathcal{H}_{IS}^0(t'), S_y(t)] \\ &\quad + i\gamma \omega_1 \text{Tr} [\mathcal{H}_0, v(t'')] [v(t'), S_y(t)] + O(\omega_1^3). \end{aligned} \quad (57)$$

The first term in (57) can be written as

$$\text{Tr} S_y(t'') [\mathcal{H}_{IS}^0(t'), S_y(t)] = \text{Tr} [S_y(t), S_y(t'')] \mathcal{H}_{IS}^0(t').$$

This term is zero for the same reason that equation (53) was zero. The second term in (57) can be written as

$$\text{Tr} [I_z, \mathcal{H}_{IS}^0(t'')] [S_x(t'), S_y(t)] = \text{Tr} [S_x(t'), S_y(t), I_z] \mathcal{H}_{IS}^0(t'') = 0$$

since

$$\left[[S_x(t'), S_y(t)], I_z \right] = 0 .$$

The third term in equation (57) is easily seen to be zero by applying the unitary operator $e^{i\pi S_z}$ to the argument of the trace. Since S_z commutes with I_z and $\mathcal{H}_{IS}^0(t)$, the rotation sends $S_y(t)$ into $-S_y(t)$ with the result that

$$\text{Tr} \left[I_z, \mathcal{H}_{IS}^0(t'') \right] \left[\mathcal{H}_{IS}^0(t'), S_y(t) \right] = -\text{Tr} \left[I_z, \mathcal{H}_{IS}^0(t'') \right] \left[\mathcal{H}_{IS}^0(t'), S_y(t) \right] = 0. \quad (58)$$

The fourth term in equation (57) when integrated over t'' becomes

$$\begin{aligned} i\gamma\omega_1 \int dt'' \text{Tr} \left[\mathcal{H}_0, V(t'') \right] \left[V(t'), S_y(t) \right] &= \gamma\omega_1 \text{Tr} \left\{ V(t') - V(0) \right\} \left[V(t'), S_y(t) \right] \\ &= \gamma\omega_1 \text{Tr} \left[V(t'), V(t') \right] S_y(t) \\ &\quad - \gamma\omega_1 \text{Tr} V(t') \left[S_y(t), V \right] \quad (59) \end{aligned}$$

The first term above is obviously zero, and the second term can be expanded to give

$$\begin{aligned} \omega_1 \text{Tr} V(t') \left[S_y(t), V \right] &= \omega_1^2 \text{Tr} \left\{ \left[S_y(t), S_x \right] \mathcal{H}_{IS}^0(t') + \left[S_x(t'), S_y(t) \right] \mathcal{H}_{IS}^0 \right\} \\ &\quad + \omega_1 \text{Tr} S_y(t) \left[\mathcal{H}_{IS}^0, \mathcal{H}_{IS}^0(t') \right] + 0 (\omega_1^3) . \end{aligned}$$

The first term on the right hand side is zero for the same reason that equation (53) was zero and the second term is zero using the identical argument leading to equation (58). Therefore, to order of ω_1^3 , $C_3 = 0$.

C_4 can be evaluated using arguments identical with those used in evaluating C_1 , C_2 , and C_3 , along with the condition that the terms of the order of ω_1^3 and ϵ^3 and higher are neglected. The result is

$$\begin{aligned}
C_4 = & -\Delta\omega_1^2 (\alpha - \gamma) \text{Tr}[S_y(t'''), \mathcal{H}_{IS}^{\circ}(t'')] [\mathcal{H}_{IS}^{\circ}(t'), S_y(t)] \\
& + i\omega_n\omega_1^2 (\beta - \gamma) \left\{ \text{Tr} \left[[I_z, \mathcal{H}_{IS}^{\circ}(t''')], S_x(t'') \right] [\mathcal{H}_{IS}^{\circ}(t'), S_y(t)] \right. \\
& \left. + \text{Tr} \left[[I_z, \mathcal{H}_{IS}^{\circ}(t''')], \mathcal{H}_{IS}^{\circ}(t'') \right] [S_x(t'), S_y(t)] \right\} \quad (60)
\end{aligned}$$

It is now assumed that each nuclear spin interacts with only one electron. For dilute systems, this is an excellent approximation. Thus the sample is broken up into N equivalent "spheres of influence," each containing one electron and $\frac{n}{N}$ protons. In this approximation, one has

$$\mathcal{H}_{IS}^{\circ} = S_z \sum_{j=1}^{\frac{n}{N}} \epsilon_j I_j^+ + S_z \sum_{j=1}^{\frac{n}{N}} \epsilon_j^* I_j^- \quad (61)$$

where the summation is over one sphere of influence, and ϵ_j is for the j^{th} proton referenced to an electron at the center of the sphere.

Integrating C_4 as indicated in equation (44) yields

$$\begin{aligned}
\int C_4 dt &= -\Delta\omega_1^2 (\alpha - \gamma) \text{Tr} \sum_{j=1}^{\frac{n}{N}} |\epsilon_j|^2 I_j^+ I_j^- \int_0^t dt' \int_0^{t'} dt'' \int_0^{t''} dt''' \\
&\times S_X(t''') S_X(t) \left[e^{i\omega_n (t'' - t')} + e^{-i\omega_n (t'' - t')} \right] \\
&+ i\omega_n \omega_1^2 (\beta - \gamma) \text{Tr} \sum_{j=1}^{\frac{n}{N}} |\epsilon_j|^2 I_j^+ I_j^- \int_0^t dt' \int_0^{t'} dt'' \int_0^{t''} dt''' \\
&\times S_Y(t''') S_X(t) \left[e^{i\omega_n (t''' - t')} - e^{-i\omega_n (t''' - t')} \right]. \quad (62)
\end{aligned}$$

We define $I(\omega_n)$ as

$$I(\omega_n) = \int_0^t dt' \int_0^{t'} dt'' e^{i\omega_n (t'' - t')} \int_0^{t''} dt''' S_X(t''') S_X(t)$$

and integrate this expression by parts

$$\begin{aligned}
I(\omega_n) &= \frac{1}{i\omega_n} \int_0^t dt' \left\{ e^{i\omega_n (t'' - t')} \int_0^{t''} dt''' S_X(t''') S_X(t) \Big|_{t''=0}^{t''=t'} \right. \\
&\quad \left. - \int_0^{t'} dt'' e^{i\omega_n (t'' - t')} S_X(t'') S_X(t) \right\},
\end{aligned}$$

which reduces to

$$\begin{aligned}
I(\omega_n) &= \frac{1}{i\omega_n} \int_0^t dt' \int_0^{t'} dt'' S_x(t'') S_x(t) \\
&\quad - \frac{1}{i\omega_n} \int_0^t dt' \int_0^{t'} dt'' e^{i\omega_n(t'' - t')} S_x(t'') S_x(t) .
\end{aligned}$$

Integrating the second term on the right in the same manner,

$$\begin{aligned}
I(\omega_n) &= \frac{1}{i\omega_n} \int_0^t dt' \int_0^{t'} dt'' S_x(t'') S_x(t) \\
&\quad - \frac{1}{\omega_n^2} \int_0^t dt' e^{i\omega_n(t' - t)} S_x(t') S_x(t) \\
&\quad + \frac{1}{\omega_n^2} \int_0^t dt' S_x(t') S_x(t) .
\end{aligned}$$

The first term on the right of equation (62) is

$$\begin{aligned}
&-\Delta\omega_1^2 (\alpha - \gamma) \text{Tr} \sum_{j=1}^{\frac{n}{N}} |\epsilon_j|^2 I_j^+ I_j^- \left\{ I(\omega_n) + I(-\omega_n) \right\} = \\
&= -\frac{2\Delta\omega_1^2}{\omega_n^2} (\alpha - \gamma) \text{Tr} \sum_{j=1}^{\frac{n}{N}} |\epsilon_j|^2 I_j^+ I_j^- \int_0^t dt' \tilde{S}_x(t' - t) S_x \cos \Delta(t' - t) \\
&\quad + \frac{\Delta\omega_1^2}{\omega_n^2} (\alpha - \gamma) \text{Tr} \sum_{j=1}^{\frac{n}{N}} |\epsilon_j|^2 I_j^+ I_j^- \\
&\quad \times \int_0^t dt' \tilde{S}_x(t' - t) S_x \left[\cos(\omega_n + \Delta)(t' - t) + \cos(\omega_n - \Delta)(t' - t) \right] .
\end{aligned} \tag{63}$$

We use the same procedure to evaluate the second term on the right of equation (62) as was used to obtain equation (63), and assume that

$|\epsilon_j|^2$ may be replaced by an average over the sphere of influence of the electron, i.e., an ϵ^2 such that

$$\epsilon^2 = \frac{N}{n} \sum_{j=1}^{\frac{n}{N}} |\epsilon_j|^2 . \quad (64)$$

In section II F, we evaluate ϵ^2 for the conditions corresponding to our experiments. Equation (62) becomes

$$\begin{aligned} \int C_4 dt &= -\Delta (\alpha - \gamma) \frac{n}{N} \frac{2\epsilon^2}{\omega_n^2} W^0(\Delta) (\text{Tr } S_z^2) \\ &+ \Delta (\alpha - \gamma) \frac{n}{N} \left[W^-(\omega_n - \Delta) + W^+(\omega_n + \Delta) \right] \text{Tr } S_z^2 \\ &- \omega_n (\beta - \gamma) \frac{n}{N} \left[W^-(\omega_n - \Delta) - W^+(\omega_n + \Delta) \right] \text{Tr } S_z^2 \quad (65) \end{aligned}$$

where

$$W^0(\Delta) = \frac{\omega_1^2}{2} g(\Delta) , \quad (66)$$

$$W^\pm(\omega_n \pm \Delta) = \frac{\epsilon^2}{\omega_n^2} \frac{\omega_1^2}{2} g(\omega_n \pm \Delta) \quad (67)$$

The electron spin resonance absorption line shape function $g(\omega)$ is defined as

$$g(\omega) = \frac{2 \operatorname{Tr} \int_0^{\infty} d\tau \tilde{S}_x(\tau) S_x \cos \omega\tau}{\operatorname{Tr} S_z^2} \quad (68)$$

and normalized such that

$$\int_{-\infty}^{\infty} d\omega g(\omega) = 2\pi .$$

The fact that

$$\frac{\operatorname{Tr} I_j^+ I_j^- \int_0^{\infty} d\tau \tilde{S}_x(\tau) S_x \cos \omega\tau}{\operatorname{Tr} S_z^2} = \frac{1}{2} \frac{\operatorname{Tr} \int_0^{\infty} d\tau \tilde{S}_x(\tau) S_x \cos \omega\tau}{\operatorname{Tr} S_z^2}$$

was used to obtain equation (65) from equation (63). W^0 and W^{\pm} are the transition probabilities per unit time associated with the allowed electron spin resonance transition and with the solid effect transitions, respectively.

Combining equation (44) with equations (56) and (65)-(68) leads to

$$\begin{aligned} \frac{d\alpha}{dt} = & - \left(1 - \frac{n}{N} \frac{2\epsilon^2}{\omega_n^2} \right) W^0(\Delta) (\alpha - \gamma) \\ & + \frac{n}{N} \frac{1}{\Delta} W^-(\omega_n - \Delta) \left\{ \omega_n \beta - \Delta\alpha - (\omega_n - \Delta)\gamma \right\} \\ & - \frac{n}{N} \frac{1}{\Delta} W^+(\omega_n + \Delta) \left\{ \omega_n \beta + \Delta\alpha - (\omega_n + \Delta)\gamma \right\} \end{aligned} \quad (69)$$

where $\frac{n}{N} \frac{2\epsilon^2}{\omega_n^2}$ is a correction factor to the allowed transition probability per unit time due to the C_4 term in the perturbation expansion. Since it is usually much less than unity, we drop it from this point on. The terms α , β , and γ in equation (69) are rigorously $\alpha(0)$, $\beta(0)$, and

$\gamma(0)$. For times t satisfying equation (8), they are approximately equal to $\alpha(t)$, $\beta(t)$, and $\gamma(t)$, respectively, and we use this approximation henceforth.

C. Derivation of the Equation of Motion for the
Nuclear Zeeman Inverse Spin Temperature, $\beta(t)$

The derivation of the equation of motion for $\beta(t)$ is similar to the derivation of the equation of motion for $\alpha(t)$. Starting from equations (39) and (43), we get

$$\begin{aligned}
 -\omega_n (\text{Tr } I_z^2) \frac{d\beta}{dt} &= i\eta \text{Tr} [\rho^R, V(t)] I_z + (i)^2 \eta \text{Tr} \int_0^t dt' \left[[\rho^R, V(t')], V(t) \right] I_z \\
 &+ (i)^3 \eta \text{Tr} \int_0^t dt' \int_0^{t'} dt'' \left[\left[[\rho^R, V(t'')], V(t') \right], V(t) \right] I_z \\
 &+ (i)^4 \eta \text{Tr} \int_0^t dt' \int_0^{t'} dt'' \int_0^{t''} dt''' \\
 &\times \left[\left[\left[[\rho^R, V(t''')], V(t'') \right], V(t') \right], V(t) \right] I_z + \dots \quad (70)
 \end{aligned}$$

We define traces analogous to the C 's of equation (45)

$$\begin{aligned}
 C_1' &= \eta \text{Tr} [\rho^R, V(t)] I_z \\
 C_2' &= \eta \text{Tr} \left[[\rho^R, V(t')], V(t) \right] I_z \\
 C_3' &= \eta \text{Tr} \left[\left[[\rho^R, V(t'')], V(t') \right], V(t) \right] I_z \\
 C_4' &= \eta \text{Tr} \left[\left[\left[[\rho^R, V(t''')], V(t'') \right], V(t') \right], V(t) \right] I_z \cdot \quad (71)
 \end{aligned}$$

C_1' and C_3' are easily shown to be zero. Evaluating C_2'

$$\begin{aligned} C_2' &= \eta \text{Tr} [\rho^R, V(t')] [V(t), I_z] \\ &= -(\beta - \gamma) \omega_n \text{Tr} [I_z, \mathcal{H}_{IS}^O(t')] [\mathcal{H}_{IS}^O(t), I_z] \end{aligned}$$

where the other terms are zero.

Using equation (27), carrying out the commutation relations and integrating C_2' as indicated in equation (70), we get

$$\begin{aligned} \int dt' C_2' &= -\omega_n (\beta - \gamma) \text{Tr} \sum_{i,k=1}^N \sum_{j=1}^n \epsilon_{ij} \epsilon_{kj}^* I_j^+ I_j^- \\ &\quad \times \int_{-t}^t d\tau S_{zi} \tilde{S}_{zk}(\tau) e^{-i\omega_n \tau} . \end{aligned}$$

The product $S_{zi} \tilde{S}_{zk}(\tau)$ is related to the correlation function for the z-component of the individual electron spins, which involves a correlation time of the order of T_{2e} . The limits on the integral may then be taken as infinity. This expression reduces to

$$\int dt' C_2' = -\omega_n (\beta - \gamma) (\text{Tr} I_z^2) W_1 \quad (72)$$

where

$$W_1 = \frac{1}{2} \frac{N}{n} \frac{\text{Tr} \sum_{j=1}^n \sum_{i,k=1}^N \epsilon_{ij} \epsilon_{kj}^* \int_{-\infty}^{\infty} d\tau S_{zi} \tilde{S}_{zk}(\tau) e^{-i\omega_n \tau}}{\text{Tr} S_z^2} . \quad (73)$$

We now use the sphere of influence model to deduce an estimate for equation (73). In this limit only $i = k$ terms will contribute significantly to equation (73) and one gets

$$W_1 = \frac{\epsilon^2}{2} \frac{\text{Tr} \sum_{i=1}^N \int_{-\infty}^{\infty} d\tau S_{zi} \tilde{S}_{zi}(\tau) e^{-i\omega_n \tau}}{\text{Tr} S_z^2},$$

where ϵ^2 was defined in equation (64). We now assume the approximation²⁵

$$\text{Tr} \sum_{i=1}^N \int_{-\infty}^{\infty} d\tau S_{zi} \tilde{S}_{zi}(\tau) e^{-i\omega_n \tau} \approx \text{Tr} \int_{-\infty}^{\infty} d\tau S_x \tilde{S}_x(\tau) e^{-i\omega_n \tau}.$$

Using equation (68) we then have

$$W_1 \approx \frac{\epsilon^2}{2} g(\omega_n). \quad (74)$$

If one assumes a Lorentzian lineshape,²⁶ equation (74) leads to the same result as reference 25. W_1 as defined by equation (73) is the transition probability per unit time resulting from the fluctuation of the z-component of the electron spins due to the electron dipole-dipole (\mathcal{H}_{SS}^0) interaction. The effect that this term has on the nuclear relaxation has been discussed in reference 25.

C_4' is found using the same arguments used to obtain equation (60).

$$\begin{aligned}
C_4' = & -i\omega_1^2 \Delta(\alpha - \gamma) \text{Tr} \left\{ \left[\left[S_y(t'''), S_x(t'') \right], \mathcal{H}_{IS}^0(t') \right] \left[\mathcal{H}_{IS}^0(t), I_z \right] \right. \\
& + \left. \left[\left[S_y(t'''), \mathcal{H}_{IS}^0(t'') \right], S_x(t') \right] \left[\mathcal{H}_{IS}^0(t), I_z \right] \right\} \\
& - \omega_n \omega_1^2 (\beta - \gamma) \text{Tr} \left[\left[\left[I_z, \mathcal{H}_{IS}^0(t''') \right], S_x(t'') \right], S_x(t') \right] \left[\mathcal{H}_{IS}^0(t), I_z \right]
\end{aligned}$$

Making the same assumptions which led to equation (61), and integrating C_4' as indicated by equation (70) yields

$$\begin{aligned}
\int dt C_4' = & i\Delta(\alpha - \gamma) \omega_1^2 \text{Tr} \sum_{j=1}^{\frac{n}{N}} |\epsilon_j|^2 I_j^+ I_j^- \int_0^t dt' \int_0^{t'} dt'' \int_0^{t''} dt''' \\
& \times S_x(t''') S_y(t') \left(e^{i\omega_n(t''-t)} - e^{-i\omega_n(t''-t)} \right) \\
& - \omega_n (\beta - \gamma) \omega_1^2 \text{Tr} \sum_{j=1}^{\frac{n}{N}} |\epsilon_j|^2 I_j^+ I_j^- \int_0^t dt' \int_0^{t'} dt'' \int_0^{t''} dt''' \\
& \times S_y(t'') S_y(t') \left(e^{i\omega_n(t'''-t)} + e^{-i\omega_n(t'''-t)} \right). \quad (75)
\end{aligned}$$

Integrating by parts as done before, and using equations (64), (67), and (68), equation (75) becomes

$$\int dt C_4' = -\Delta(\text{Tr } I_z^2) (W^- - W^+) (\alpha - \gamma) + \omega_n (\text{Tr } I_z^2) (W^- + W^+) (\beta - \gamma). \quad (76)$$

Combining equations (72) and (76) with equation (70) yields

$$\begin{aligned} \frac{d\beta}{dt} = & -W_1(\beta - \gamma) - \frac{1}{\omega_n} W^- (\omega_n - \Delta) \left\{ \omega_n \beta - \Delta \alpha - (\omega_n - \Delta) \gamma \right\} \\ & - \frac{1}{\omega_n} W^+ (\omega_n + \Delta) \left\{ \omega_n \beta + \Delta \alpha - (\omega_n + \Delta) \gamma \right\} . \end{aligned} \quad (77)$$

D. Derivation of the Equation of Motion for the
Electron Dipole-Dipole Inverse
Temperature, $\gamma(t)$

The derivation of the equation of motion for the electron dipole-dipole inverse temperature, $\gamma(t)$, can be accomplished using the fact that energy is conserved in the rotating reference frame for times t satisfying equation (8), provided that

$$\langle \mathcal{H}_0 \rangle \gg \langle V \rangle ,$$

where \mathcal{H}_0 and V are defined in equations (31) and (32), respectively.

Then

$$\frac{d\langle \mathcal{H}_0 \rangle}{dt} = 0 = \text{Tr} \left(\Delta S_z + \omega_n I_z + \mathcal{H}_{SS}^0 \right) \frac{\partial \rho^R}{\partial t} ,$$

so that

$$+\Delta^2 \left(\text{Tr} S_z^2 \right) \frac{d\alpha}{dt} + \omega_n^2 \left(\text{Tr} I_z^2 \right) \frac{d\beta}{dt} + \text{Tr} \left(\mathcal{H}_{SS}^0 \right)^2 \frac{d\gamma}{dt} = 0 . \quad (78)$$

Substituting equations (69) and (77) into (78) and using

$(\text{Tr} I_z^2 / \text{Tr} S_z^2) = n/N$, we get

$$\begin{aligned}
\frac{d\gamma}{dt} = & + \frac{n}{N} \frac{\omega_n^2}{\omega_L^2} W_1 (\beta - \gamma) + \frac{\Delta^2}{\omega_L^2} W^0(\Delta) (\alpha - \gamma) \\
& + \frac{n}{N} \frac{(\omega_n - \Delta)}{\omega_L^2} W^- (\omega_n - \Delta) \left\{ \omega_n \beta - \Delta \alpha - (\omega_n - \Delta) \gamma \right\} \\
& + \frac{n}{N} \frac{(\omega_n + \Delta)}{\omega_L^2} W^+ (\omega_n + \Delta) \left\{ \omega_n \beta + \Delta \alpha - (\omega_n + \Delta) \gamma \right\} \quad (79)
\end{aligned}$$

where

$$\omega_L^2 = \frac{\text{Tr}(\mathcal{H}_{SS}^0)^2}{\text{Tr} S_z^2} .$$

The term ω_L^2 is related to the linewidth of the electron spin resonance line. It is found to be^{14,26}

$$\omega_L^2 = \frac{1}{3} M_2$$

where M_2 is the second moment of the electron spin resonance line.

E. Effects of the Lattice Reservoir

The effect of the lattice vibrations (phonons) is introduced by assuming that each spin-lattice relaxation process takes place exponentially with a characteristic spin-lattice relaxation time, and that these processes may be added to the equations of evolution for α , β , and γ .^{8, 14, 16, 24, 26} Thus equations (69), (77), and (79) become

$$\begin{aligned} \frac{d\alpha}{dt} = & -W^0(\Delta) (\alpha - \gamma) + \frac{n}{N} \frac{1}{\Delta} W^-(\omega_n - \Delta) \left\{ \omega_n \beta - \Delta\alpha - (\omega_n - \Delta)\gamma \right\} \\ & - \frac{n}{N} \frac{1}{\Delta} W^+(\omega_n + \Delta) \left\{ \omega_n \beta + \Delta\alpha - (\omega_n + \Delta)\gamma \right\} - \frac{1}{T_e} \left(\alpha - \frac{\omega_e}{\Delta} \beta_L \right) \end{aligned} \quad (80a)$$

$$\begin{aligned} \frac{d\beta}{dt} = & -W_1(\beta - \gamma) - \frac{1}{\omega_n} W^-(\omega_n - \Delta) \left\{ \omega_n \beta - \Delta\alpha - (\omega_n - \Delta)\gamma \right\} \\ & - \frac{1}{\omega_n} W^+(\omega_n + \Delta) \left\{ \omega_n \beta + \Delta\alpha - (\omega_n + \Delta)\gamma \right\} - \frac{1}{T_n} (\beta - \beta_L) \end{aligned} \quad (80b)$$

$$\begin{aligned} \frac{d\gamma}{dt} = & \frac{\Delta^2}{\omega_L^2} W^0(\Delta) (\alpha - \gamma) + \frac{n}{N} \frac{\omega_n^2}{\omega_L^2} W_1(\beta - \gamma) \\ & + \frac{n}{N} \frac{(\omega_n - \Delta)}{\omega_L^2} W^-(\omega_n - \Delta) \left\{ \omega_n \beta - \Delta\alpha - (\omega_n - \Delta)\gamma \right\} \\ & + \frac{n}{N} \frac{(\omega_n + \Delta)}{\omega_L^2} W^+(\omega_n + \Delta) \left\{ \omega_n \beta + \Delta\alpha - (\omega_n + \Delta)\gamma \right\} - \frac{1}{T_D} (\gamma - \beta_L) \end{aligned} \quad (80c)$$

where T_e , \bar{T}_n (see section II F), and T_D , are the spin-lattice relaxation times of the electron-Zeeman, nuclear-Zeeman, and electron dipole-dipole reservoirs,^{8, 14, 16, 24, 26} respectively, and β_L is the inverse temperature of the lattice. Note that the electron-Zeeman inverse temperature does not approach the inverse lattice temperature,

but the "colder" temperature $\frac{\omega_e}{\Delta} \beta_L$. This is a result of the transformation to the rotating frame which affects the electron Zeeman interaction, but does not affect the nuclear Zeeman and the secular electron dipole-dipole interactions.

F. Nuclear Spin Diffusion

The nuclear dipole-dipole interaction, \mathcal{H}_{II} , was ignored in the derivation of the kinetic equations governing the solid effect. This interaction becomes important if $N \ll n$, for there will be large regions in the solid where the electron-nuclear dipole-dipole interaction is very small compared to the nuclear dipole-dipole interaction. The nuclear magnetization in these regions will be spatially transported by energy conserving transitions resulting from the terms $I_j^- I_k^+$ of \mathcal{H}_{II} . This process is called nuclear spin diffusion. Only a brief discussion of spin diffusion in the rapid diffusion limit will be given here and will closely follow the treatment given by Abragam and Borghini.¹⁴ More elaborate discussions of spin diffusion are given elsewhere.²⁷⁻³¹

Each electron can be considered to interact only with the nuclei within its sphere of influence having a radius R defined by

$$R = \left(\frac{4\pi}{3} N \right)^{-1/3}, \quad (81)$$

where N is the number of paramagnetic ions per unit volume. An important parameter is the pseudopotential radius b , which is the

distance from the electron at which a nucleus has approximately the same probability of being relaxed by the electron as of being flipped by the \mathcal{H}_{II} terms due to neighboring nuclei, and is given by²⁸

$$b = 0.68 \left(\frac{C}{D} \right)^{1/4} . \quad (82)$$

The term C is

$$C = \frac{3}{10} \gamma_e^2 \gamma_n^2 \hbar^2 \frac{T_e}{1 + \omega_n^2 T_e^2} , \quad (83)$$

and D is the diffusion constant given approximately by²⁹

$$D = \frac{1}{10} \frac{a^2}{T_{2n}} . \quad (84)$$

Here a is the average distance between nuclei and T_{2n} is the nuclear spin-spin relaxation time. Another important parameter in spin diffusion theory is the diffusion barrier radius b_0 , defined¹⁶ as the distance from the paramagnetic ion at which the magnetic field at the site of the nuclear spin due to the ion is equal to the nuclear line-width and given very approximately as

$$b_0 = a \left(\frac{\gamma_e}{\gamma_n} \right)^{1/3} . \quad (85)$$

The regime of "rapid diffusion"^{28,30} defined by the inequality

$$a, b \ll b_0 \ll R, \quad (86)$$

corresponds to the conditions for the crystals and temperatures reported in this thesis.

Detailed calculations^{14,28,29,30} show that in the limit of rapid diffusion, equation (80b) can be written as

$$\frac{d\bar{\beta}}{dt} = -W (\bar{\beta} - \beta_0) \quad (87)$$

where

$$W = \bar{W}_1 + \bar{W}^+ (\omega_n + \Delta) + \bar{W}^- (\omega_n - \Delta) + \frac{1}{T_n} \quad (88)$$

and

$$\beta_0 = \frac{1}{W} \left\{ \left(\frac{1}{T_n} \right) \beta_L + \frac{\Delta}{\omega_n} (\bar{W}^- - \bar{W}^+) \alpha + \left(\bar{W}_1 + \frac{\omega_n - \Delta}{\omega_n} \bar{W}^- + \frac{\omega_n + \Delta}{\omega_n} \bar{W}^+ \right) \gamma \right\} \quad (89)$$

The bars correspond to angular and radial averages within a spherical shell whose radius r is bounded by

$$b_0 \leq r \leq R.$$

In this limit and within these approximations, ϵ^2 , defined in equation (64), becomes

$$\epsilon^2 = \frac{3}{10} \gamma_e^2 \gamma_n^2 \frac{\hbar^2}{b_0^3 R^3}, \quad (90)$$

and is the appropriate expression to use in equations (67), (74), and all three equations (80). Henceforth, we assume that this is done, and omit the bars over W_1 and W_1^\pm , but not over \bar{T}_n . One can show that^{14,30,31}

$$\frac{1}{\bar{T}_n} = \frac{4\pi}{3} \frac{NC}{b_0^3} + \frac{1}{T_{nL}}. \quad (91)$$

The first term is due to nuclear relaxation by the desired paramagnetic impurity (the samarium ions, in our case), and the second term is "leakage" relaxation by other impurities and by other modes of spin-lattice interaction. The physical picture is that the relaxation and rf transitions caused by W tend to drive the inverse temperature $\bar{\beta}$ to a steady state value given by β_0 and at the same time the spin diffusion mechanism attempts to keep the total nuclear magnetization spatially homogeneous.

It is left to determine the measured spin-lattice relaxation rate, $1/T_n$. In the absence of any radio frequency fields, equation (87) can be written as

$$\frac{d\bar{\beta}}{dt} = -W_1 (\bar{\beta} - \gamma) - \left(\frac{1}{\bar{T}_n} \right) (\bar{\beta} - \beta_L). \quad (92)$$

The time evolution of γ must be taken into account also, i.e.,

$$\frac{d\gamma}{dt} = -\left(\frac{n}{N} \frac{\omega_n^2}{\omega_L^2}\right) W_1 (\gamma - \beta) - \frac{1}{T_D} (\gamma - \beta_L). \quad (93)$$

The general solution for $\bar{\beta}$ exhibits two time constants. There are several limiting cases for which the longer time constant can be easily evaluated; this will be the measured T_n . One limit is

$$W_1 \ll \left(\frac{1}{T_n}\right),$$

in which case

$$T_n = \bar{T}_n.$$

A second limit is the situation in which

$$\left(\frac{1}{T_D}\right), \left(\frac{n\omega_n^2}{N\omega_L^2}\right) W_1 \gg W_1, \left(\frac{1}{T_n}\right).$$

In this case γ will come to quasi-equilibrium (i.e., $\frac{d\gamma}{dt} \approx 0$) in times t such that

$$T_D, \left(\frac{N\omega_L^2}{n\omega_n^2}\right) W_1^{-1} \ll t \ll W_1^{-1}, \bar{T}_n.$$

Thus, equation (93) may be solved for γ , which is then substituted into equation (92). The latter can be rewritten as

$$\frac{d\bar{\beta}}{dt} = \frac{1}{T_n} (\bar{\beta} - \beta_L)$$

where

$$\frac{1}{T_n} = \frac{1}{T_n} + \frac{W_1}{1 + \frac{n\omega_n^2}{N\omega_L^2} W_1 T_D} . \quad (94)$$

If

$$1 \gg \left(\frac{n\omega_n^2}{N\omega_L^2} \right) W_1 T_D$$

equation (94) becomes

$$\frac{1}{T_n} = \frac{1}{T_n} + W_1 . \quad (95)$$

On the other hand, if

$$1 \ll \left(\frac{n\omega_n^2}{N\omega_L^2} \right) W_1 T_D ,$$

one obtains

$$\frac{1}{T_n} = \frac{1}{T_n} + \frac{N\omega_L^2}{n\omega_n^2} \frac{1}{T_D} . \quad (96)$$

Combining equations (91) and (94), we get

$$\frac{1}{T_n} = \frac{4\pi}{3} \frac{NC}{b_o^3} + \frac{1}{T_{n1}} + \frac{W_1}{1 + \frac{n\omega_n^2}{N\omega_L^2} W_1 T_D} \quad (97)$$

which is consistent with the crystals and temperatures considered in this thesis. The last term on the right side of equations (94) through (97) is a result of the coupling of the nuclear spins with the electron dipole-dipole reservoir.²⁵ We note that $1/T_D$ is often taken¹⁴ to be $2/T_e$.

G. Theoretical Dynamic Nuclear Polarization Results

The dynamic nuclear polarization, usually expressed in terms of the steady-state enhancement E defined as

$$E = \frac{\bar{\beta}}{\beta_L},$$

can be deduced from equations (80) and (87) - (89) by setting all the time derivatives equal to zero and solving for $\bar{\beta}$. The cumbersome general expression can be deduced from Cramer's Rule and can be found in appendix A. We find E for several limiting cases.

Consider first the case of well-resolved solid effect transitions, that is, $W^{\pm}, W_{\perp} \neq 0$; $W^{\mp}, W^0 = 0$. One finds for $(\omega_n \pm \Delta) \approx 0$ the result

$$E = \frac{1 \mp \frac{\omega_e}{\omega_n} W^{\pm} T_n}{1 + W^{\pm} T_n \left(1 + \frac{n}{N} \frac{T_e}{T_n} \right)} \quad (98)$$

where T_n is the measured nuclear spin-lattice relaxation time given in equation (97). For saturating microwave powers ($W^{\pm} T_n \gg 1$), equation (98) reduces to

$$E = \frac{\mp \frac{\omega_e}{\omega_n}}{1 + \frac{n}{N} \frac{T_e}{T_n}} \quad (99)$$

The term $\frac{n}{N} \frac{T_e}{T_n}$ has been called the leakage factor in the literature.^{12,15} If this term is small compared to unity, then equation (99) becomes

$$E = \pm \frac{\omega_e}{\omega_n} . \quad (100)$$

The nuclei have in effect been given the thermal equilibrium temperature and polarization of the electrons. This first limit, to which equation (98) applies, corresponds to the experiments reported in this thesis.

A second limit is that of unresolved solid effect transitions, ignoring all leakage factor effects. In this case, one can deduce

$$E = \frac{1 + \frac{\omega_e}{\omega_n} (W^- \bar{T}_n - W^+ \bar{T}_n) + W_1 \bar{T}_n + W^0 T_e \left[1 + \frac{\Delta^2}{\omega_L^2} \frac{T_D}{T_e} + \left(1 + \frac{\Delta \omega_e}{\omega_L^2} \frac{T_D}{T_e} \right) (W_1 \bar{T}_n + W^- \bar{T}_n + W^+ \bar{T}_n) \right]}{(1 + W_1 \bar{T}_n + W^- \bar{T}_n + W^+ \bar{T}_n) \left(1 + W^0 T_e + \frac{\Delta^2}{\omega_L^2} W^0 T_D \right)} .$$

This is the Abragam and Borghini¹⁴ result with the addition of the W_1 factors.^{16,25} At low microwave powers, this becomes

$$E \approx 1 + \frac{\omega_e}{\omega_n} \frac{(W^- - W^+) \bar{T}_n}{1 + W_1 \bar{T}_n} ,$$

whereas, for saturating levels of microwave power, one gets

$$E \approx \frac{\omega_e}{\omega_n} \frac{\omega_n \Delta}{\Delta^2 + \omega_L^2 \left(\frac{T_e}{T_D} \right)} .$$

The leakage factor corrections to these equations requires the full solution to equations (80) and (87) - (89) and is given in appendix A.

III. EXPERIMENTAL APPARATUS AND PROCEDURE

Figure 1 is a picture of the experimental apparatus used in this study. The experimental equipment consisted of a nuclear magnetic resonance (NMR) spectrometer, an electron spin resonance (ESR) spectrometer, an electromagnet, and a cryogenic system.

A. Nuclear Magnetic Resonance Spectrometer

The NMR spectrometer is shown schematically in figure 2. The NMR detector was of the "Q-meter" type. A detailed discussion of the theory of operation and of the limitations of this detector is given in reference 32. The rf oscillator was a constant voltage device, and a ramp generator was used to sweep the frequency. A "line-stretcher" was used to maintain a half wavelength line between the sample coil and the variable capacitor that made up the tank circuit of the "Q-meter." The sample coil consisted of two turns of teflon coated number 36 copper wire wound on the crystal. The coil leads were fed through a small hole drilled in the end wall of the microwave cavity and connected to the coaxial cable. Care was taken to have the plane of the sample coil parallel to the microwave magnetic field to prevent coupling of the microwave power out of the cavity through the NMR spectrometer. Standard lock-in detection was used to record the NMR spectra.

B. Electron Spin Resonance Spectrometer

The ESR spectrometer used in this experiment is shown schematically in figure 3. The spectrometer was a standard circuit employing



Figure 1.- Apparatus used in the DNP experiments.

1970

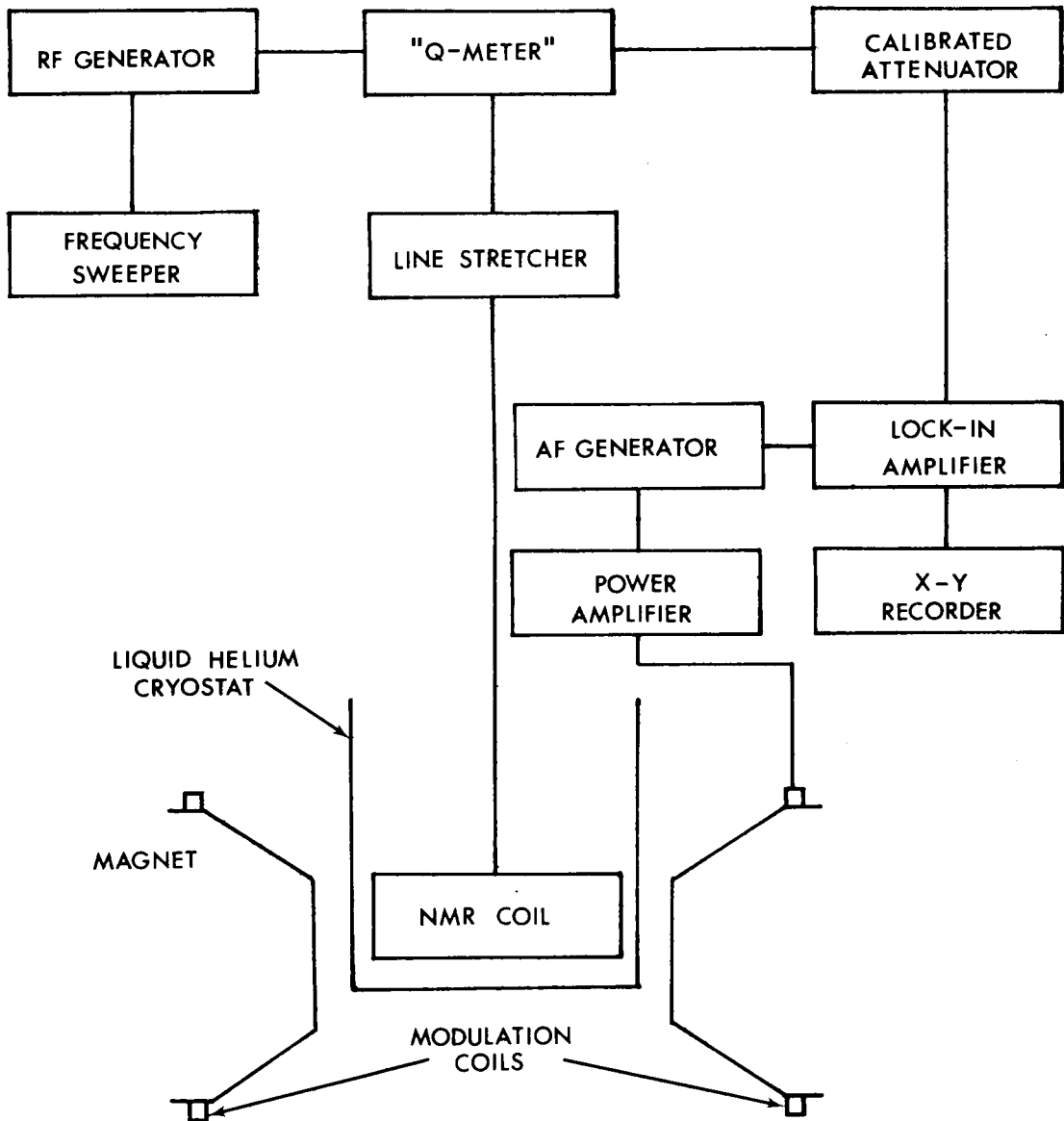


Figure 2.- Block diagram of the nuclear magnetic resonance spectrometer.

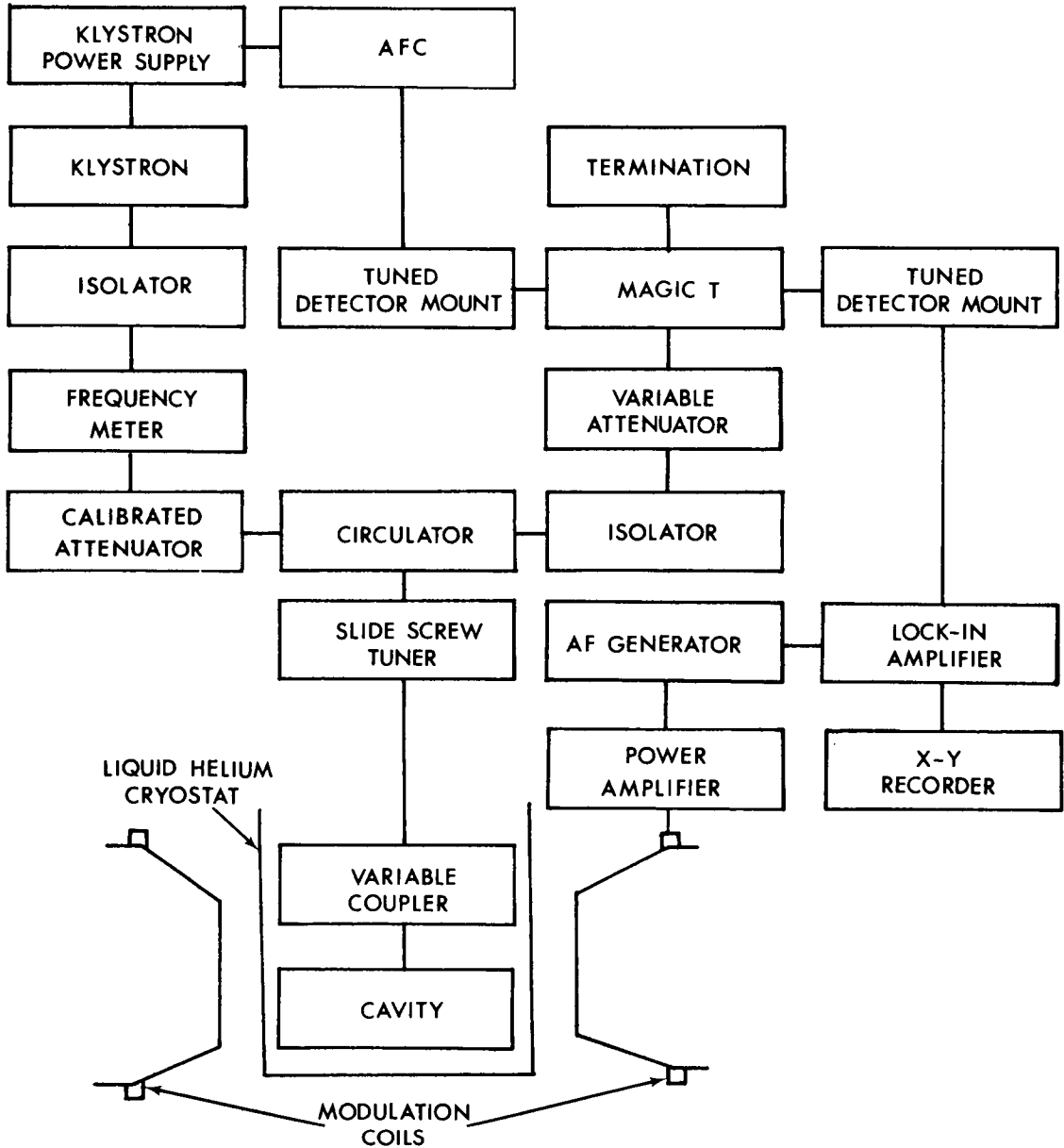


Figure 3.- Block diagram of the electron spin resonance spectrometer.

a three-port circulator to utilize all the power furnished by the klystron. The klystron was a Varian Model V58 reflex klystron rated at 500 milliwatts at X-band. The klystron frequency was locked to the resonance frequency of the sample cavity using an automatic frequency control circuit similar to the Berry and Benton circuit.³³ A sketch of the cryogenic probe containing the sample cavity and variable coupler are shown in figure 4. The sample cavity was machined from brass and gold plated and resonated in the cylindrical TE 111 mode. A wire was soldered on a diameter of the sample cavity to short one of the two degenerate resonant modes. A small cylindrical section of teflon was screwed to an end wall of the cavity and used as a crystal mount. The variable coupler used was similar to that discussed in reference ³⁴. The sample cavity and variable coupler were attached to a length of thin wall stainless steel type 304 waveguide, and this was soldered to a flange which bolted to the top of the cryostat. Standard lock-in detection was used to record the ESR spectra.

C. Magnet

The magnet employed was a Varian 23 cm electromagnet having a 6.7 cm air gap, with Fieldial^(R) and Hall probe control. Coils were positioned around the pole pieces to provide the magnetic field modulation necessary for lock-in detection of the signals.

D. Cryogenic System

The apparatus used to measure and control the temperature of the liquid helium bath is shown in figure 5. The temperature of the helium

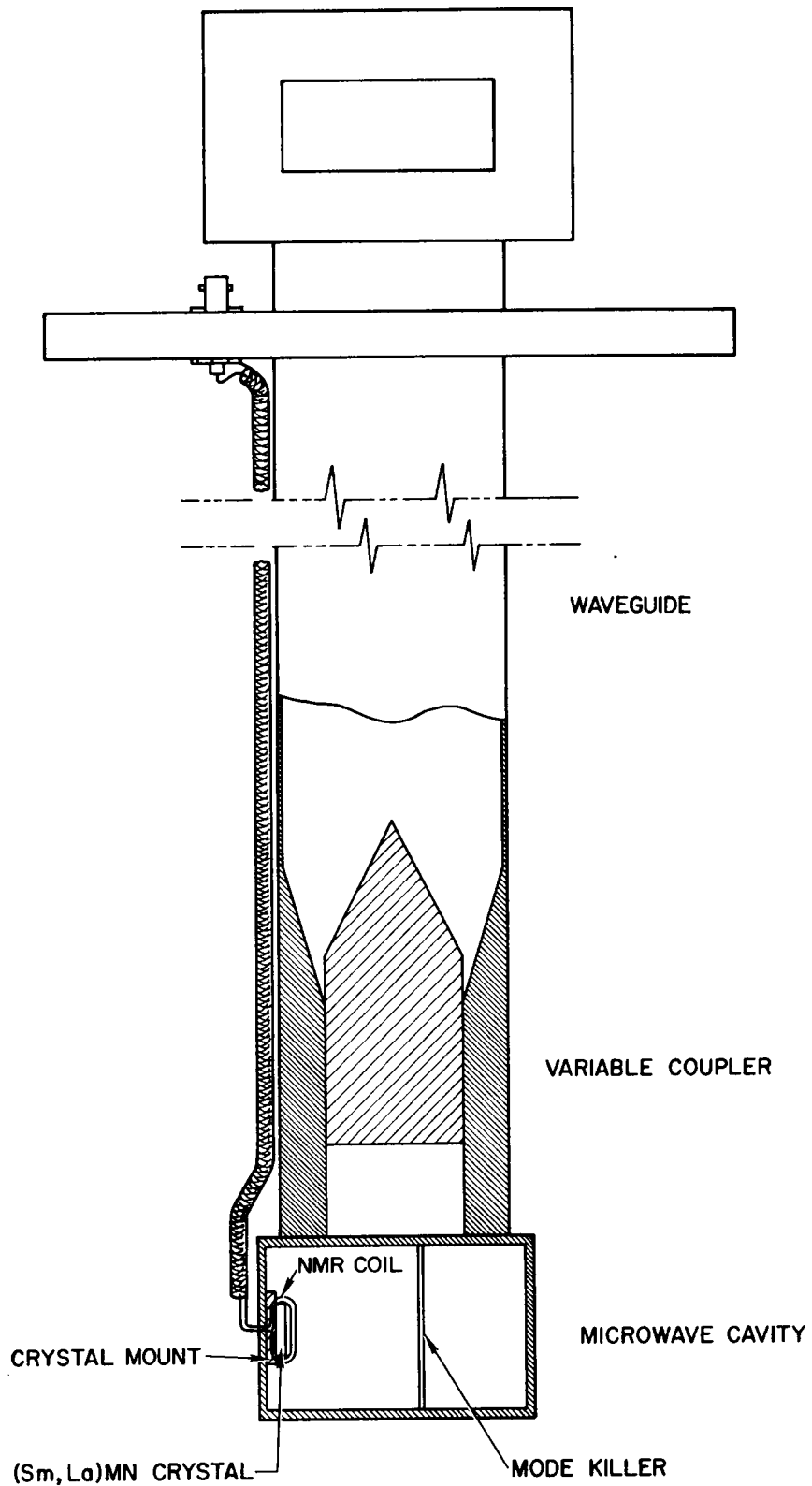


Figure 4.- Sketch of the cryogenic sample probe.

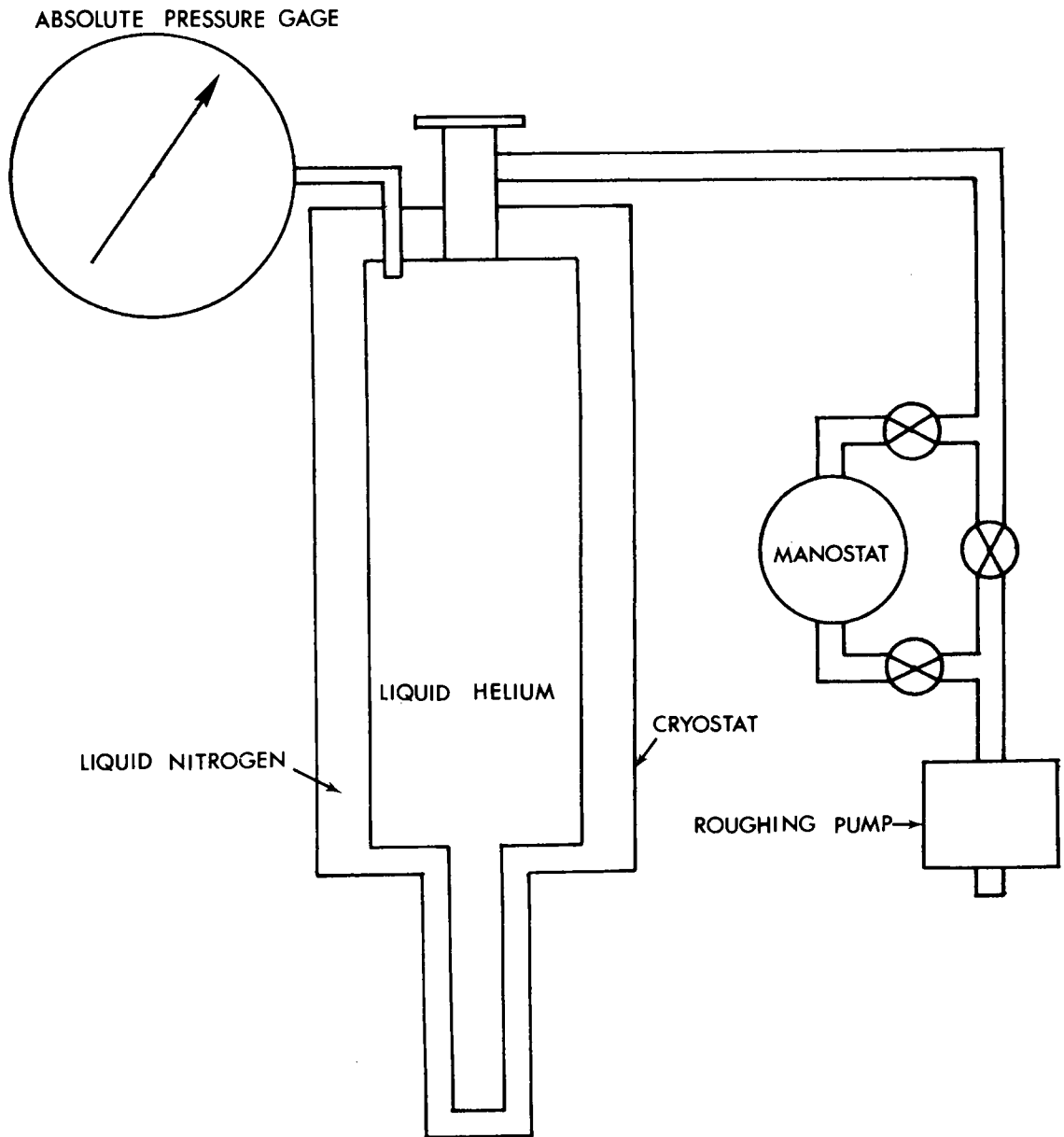
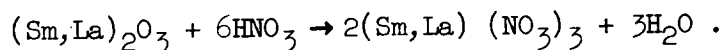


Figure 5.- Schematic of the cryogenic system.

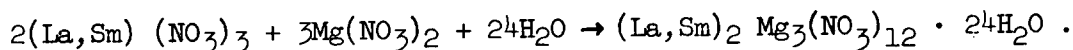
bath was monitored by measuring the vapor pressure of the liquid helium and converting the vapor pressure to temperature using the 1958 Helium-4 Temperature Scale.³⁵ Temperatures below 4.2° K were maintained in the 8 liter helium dewar by pumping over the liquid with mechanical roughing pumps having a total pumping capacity of 10 liters/sec. A constant vapor pressure was maintained by a manostat connected between the helium bath and the roughing pump as shown.

E. Sample Preparation

The samples were prepared starting with the rare earth oxides La_2O_3 and Sm_2O_3 obtained from the Lindsay Division of American Potash and Chemical Corporation. Both the La_2O_3 and Sm_2O_3 had a 99.99 percent rare earth purity. Both oxides contained the naturally occurring isotopic compositions. The rare earth nitrates were synthesized separately using reagent grade concentrated nitric acid in the reactions;



The pure rare earth nitrates were then added to reagent grade magnesium nitrate in the reactions:



The pure Sm and La double nitrate solutions were allowed to saturate at room temperature and then mixed to yield aqueous solutions of samarium doped lanthanum magnesium nitrate (Sm:LMN). The doped solutions were

poured into beakers, placed into a desiccator having concentrated sulfuric acid acting as a desiccant, and maintained at 0° C.

Single crystals of the rare earth double nitrates weighing approximately 200 mg. could be grown in about 30 hours. The growth habit is a flat hexagonal plate with the crystal symmetry axis perpendicular to the plate. The detailed crystal structure of these salts can be found elsewhere.^{8,36}

F. Experimental Procedure

Small slits were cut into the edges of the sample crystals to align the two turn NMR coil. The crystal was glued to the teflon sample mount on the end wall of the microwave cavity and the probe immersed in liquid helium. The samarium ESR line was located and recorded. The angle θ between the crystal symmetry axis and the dc magnetic field was determined and found to be approximately 7° in all but one case.

With the microwave power off, a thermal equilibrium NMR signal was recorded by sweeping frequency at a given temperature and magnetic field. Thermal equilibrium nuclear polarizations at different temperatures and magnetic fields were calculated using this result and the Brillouin function. With the dc magnetic field approximately 50 Oe below the main ESR line the microwave power was turned on and a dynamic equilibrium allowed to be established between the various reservoirs. The enhanced NMR signal was recorded by sweeping frequency. The dc magnetic field was changed and after a few nuclear spin-lattice

relaxation times the NMR spectrum again recorded. We measured the NMR derivative peak-to-peak height using magnetic field modulation with a peak-to-peak amplitude of 2.5 Oe and a frequency of 30 Hz. Because of signal-to-noise problems, the thermal equilibrium NMR measurements had a relative error of ± 20 percent, while enhanced NMR signals had a relative error of $\pm 3 - 5$ percent.

The nuclear spin-lattice relaxation times were measured by enhancing the NMR signal with microwave power, then turning the microwave power off and recording the decay of the NMR derivative peak. Any frequency drift in the rf oscillator during the measurements of T_n was corrected by monitoring the frequency and applying a correction voltage to the voltage-controlled oscillator. The data was plotted on semi-log paper and T_n determined from the slope.

IV. EXPERIMENTAL RESULTS

The experimental results for eight samarium doped lanthanum magnesium nitrate crystals are summarized in table I. The positions of the hyperfine lines of Sm^{147} and Sm^{149} were determined^{19,37} for the applied magnetic fields and frequencies listed in table I and found to be far removed from the solid effect and main ESR transitions, and thus they should have no effect on the DNP process except possibly through leakage relaxation T_{n1} .

The magnetic field H_0 reported as item 3 in the table is the magnetic field value halfway between the enhancement extremums and is assumed to be the field at which the main ESR transition occurs for the frequency reported as item 4. The value of H_0 reported is within ± 5 Oe of the value measured when the ESR transition was located and recorded. The variation of the position of the main ESR line is due to the backlash in the field control.

The angle, θ , between the crystal symmetry axis and the applied magnetic field was determined using the values

$$g_{\parallel} = 0.736 \pm 0.005$$

$$g_{\perp} = 0.363 \pm 0.10$$

reported in reference 38. The value for g_{\parallel} was measured for a number of crystals and found to have a value of 0.732. The value of g_{\perp} could not be measured due to the field strength limitations of the magnet. The parameter g of the electronic system is defined by

TABLE I. Summary of experimental parameters: Item 1 is the crystal designation; item 2 is the measured temperature in degrees Kelvin; item 3 is the magnetic field in oersteds halfway between enhancement extrema; item 4 is the microwave frequency in gigahertz used to induce the forbidden transitions; item 5 is the angle in degrees between the applied magnetic field H_0 and the crystal symmetry axis; item 6 is the electron spin-lattice relaxation time in seconds taken from reference 3; item 7 is the measured nuclear spin-lattice relaxation time unless otherwise noted; item 8 (9) is the measured derivative peak-to-peak line width in oersteds of the ESR (NMR) transition; item 10 is the satellite separation in oersteds, measured and calculated; item 11 (12) is the maximum positive (negative) enhancement measured; item 13 gives the percent dilution of samarium in the crystal solution and the measured dilution in the crystal; item 14 is the leakage factor calculated from items 6, 7, and 13; item 15 is the infinite power enhancement, calculated from the dependence of enhancement on microwave power, neglecting the leakage factor; item 16 is discussed in the text; item 17 is the enhancement corrected for leakage; and item 18 is the ideal enhancement and is discussed in the text.

	1	2	3	4	5	6	7	8
1. CRYSTAL								
2. TEMPERATURE (°K)	4.23	3.06	1.81	1.87	4.22	4.22	3.0	4.24
3. H_0 (Oe)	8915	8925	8903	8900	8952	8926	8872	8935
4. ν_e (GHz)	-----	9.112	9.130	9.121	9.155	9.156	9.118	9.120
5. θ (degrees)	-----	0	7	7	7	6	6	7
6. T_e (sec)	2.5×10^{-5}	0.0018	0.10	0.10	2.5×10^{-5}	2.5×10^{-5}	0.0015	0.10
7. T_n (sec)	42	100 ^a	250 ^a	200	15	15 ^a	100 ^a	250 ^a
8. ΔH_{pp}^e (Oe)	3.5	5.2	-----	5	5	5	5	5
9. ΔH_{pp}^n (Oe)	-----	-----	-----	13	10	12.5	10	-----
10. SATELLITE SEPARATION (Oe)								
Measured	73	74	-----	74	74	72	74	74
Calculated	-----	74.4	-----	74.2	74.6	74	74	74
11. F_{max}^+	64	78	22	38	36	23	50	17
12. F_{max}^-	64	80	-----	35	40	24	50	17
13. SAMARIUM DILUTION (%)								
Solution	20	15	15	20	20	25	25	25
Measured ^b	-----	-----	0.1	0.3	0.3	0.8	0.8	1.1
14. $(1 + n T_e / n T_n)$	-----	-----	10.6	5	1.01	1.01	1.05	2.2
15. E'	-----	117	23.8	-----	197	-----	77	-----
16. S_0	-----	0.44	0.070	-----	4.21	-----	0.52	-----
17. $E' (1 + n T_e / n T_n)$	-----	-----	245	190	199	-----	81	-----
18. E_{ideal}	240	240	240	240	240	240	240	240

^ataken from figure 11.

^bmeasured samarium concentrations were made by X-ray fluorescence.

$$g = \frac{\gamma e^{\hbar}}{\beta_M},$$

where β_M is the Bohr magneton. For axially symmetric crystals like Sm:LMN, one can show^{8,19}

$$g(\theta) = \left[g_{\parallel}^2 \cos^2\theta + g_{\perp}^2 \sin^2\theta \right]^{1/2}.$$

There was indication from the literature³⁹ that the samarium ion is highly rejected by the host lattice of LMN. A single crystal of samarium magnesium nitrate was grown and used as a standard to determine the actual concentration in the Sm:LMN using X-ray fluorescence. The solution and measured dilutions of Sm:LMN for each of the crystals is listed as item 13 in table I. The measured dilution of samarium in LMN was used to calculate the leakage factor $\frac{n}{N} \frac{T_e}{T_n}$, which occurs in the denominator of equation (98). The electron spin-lattice relaxation time T_e was calculated from the expression

$$\frac{1}{T_e} = 3.4 T + 1.3 \times 10^{-2} T^9 + 1.6 \times 10^{+10} e^{-55/T} \quad (101)$$

which was determined experimentally by Larson and Jeffries³⁹ for dilute Sm:LMN in the parallel orientation under conditions similar to ours. The crystals we used were not all in the parallel orientation when the data was taken, but T_e for Sm:LMN does not vary appreciably in this temperature range for angles $\theta \lesssim 10^\circ$.⁴⁰

A reproduction of the derivative of an ESR absorption signal is given in figure 6. Most of the crystals used in this experiment exhibited a similar asymmetry. The derivative peak-to-peak values ΔH_{pp}^e of the ESR absorption line for the crystals are listed in table I.

Figures 7 and 9 are enhancement curves for two crystals. The enhancement is the ratio of dynamic to thermal equilibrium proton polarization. The solid lines are smooth curves through the data points. Figures 8 and 10 are the variations of the peak enhancements as a function of microwave power for the same two crystals. It is evident that the peak enhancement is limited by microwave power. The enhancement versus relative microwave power data was fit by computer to the equation

$$E = E' \frac{S}{S + S_0} \quad (102)$$

This is equation (98) expressed in terms of $E (= \bar{\beta}/\beta_L)$ and E' defined as

$$E' = \frac{\frac{\omega_e}{\omega_n}}{1 + \frac{n}{N} \frac{T_e}{T_n}} \quad (103)$$

(The one (1) in the numerator of equation (98) is neglected compared to other terms in the numerator.) S is the microwave power in arbitrary units (maximum experimental power corresponds to $S = 1$), and S_0 is a constant determined in the computerized least squares fit.

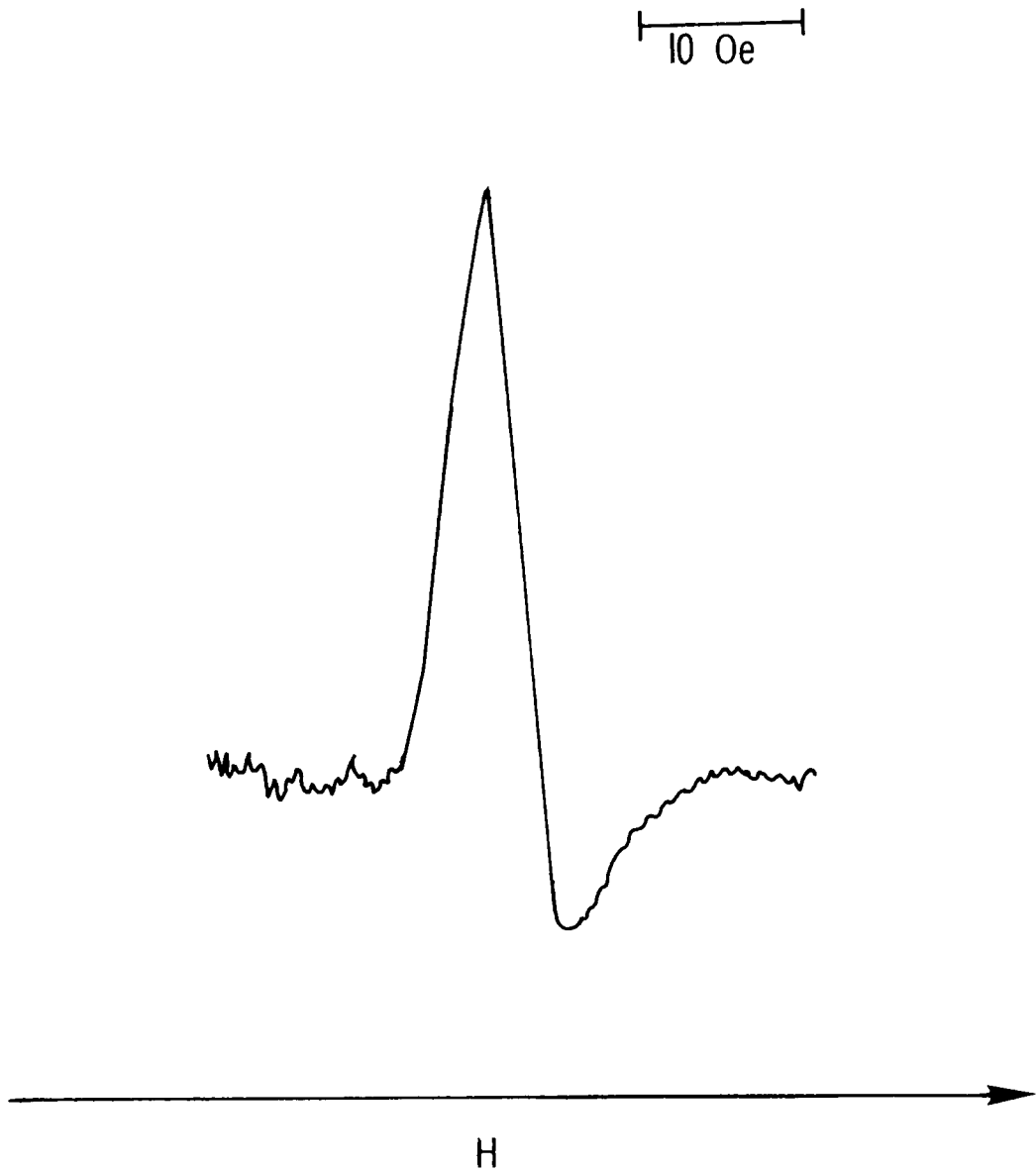


Figure 6.- The derivative of the ESR absorption line for crystal 4.

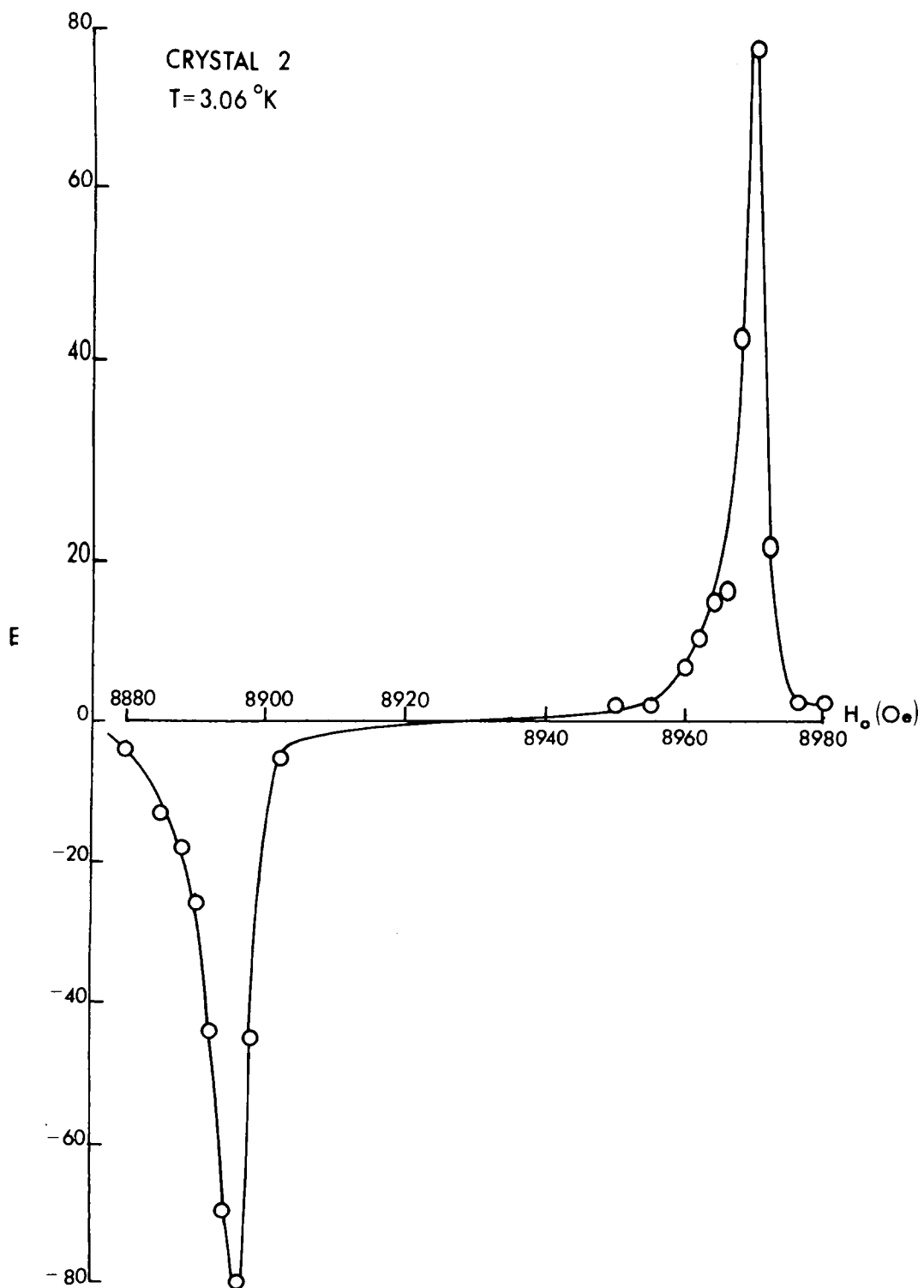


Figure 7.- Enhancement curve for crystal 2 at 3.06°K .

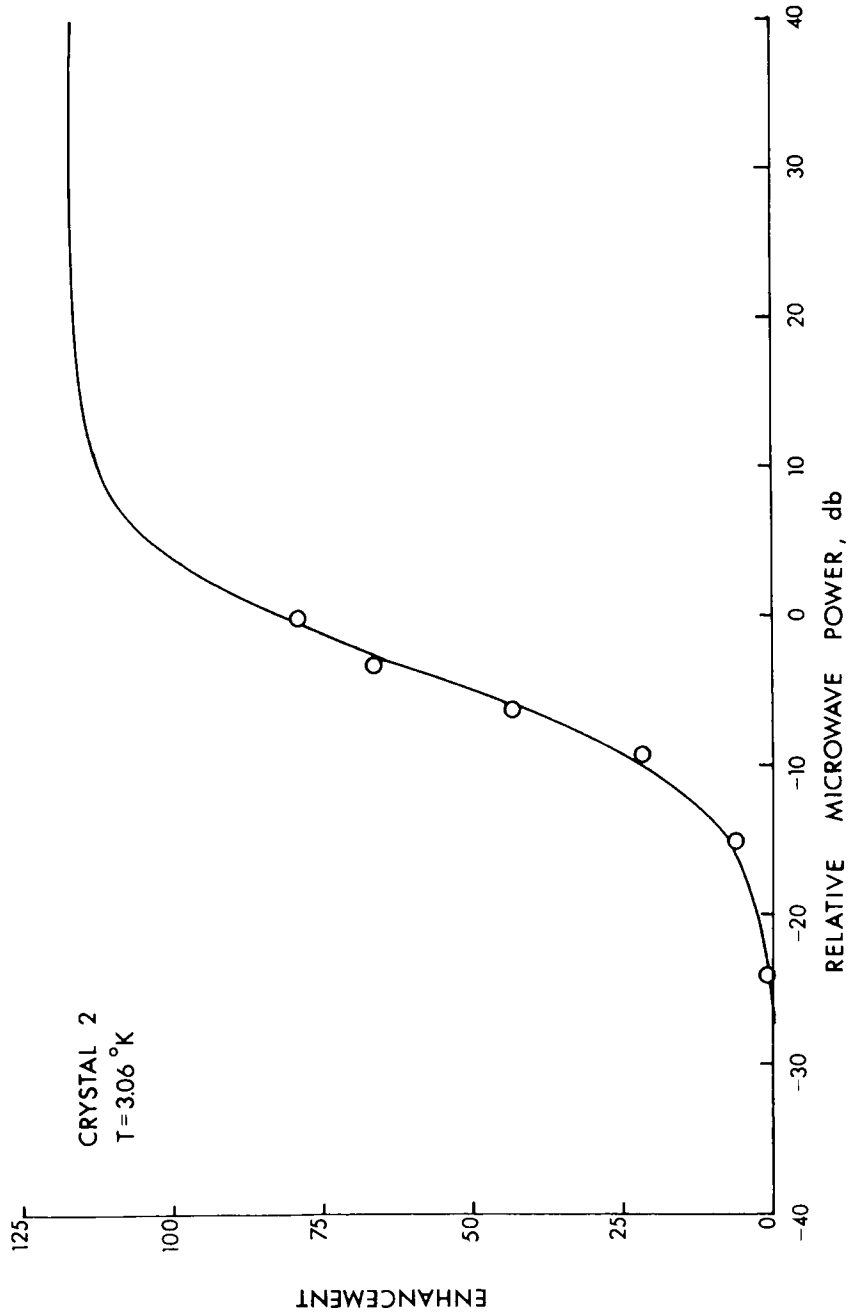


Figure 8.- Enhancement of the polarization peak as a function of relative microwave power for crystal 2.

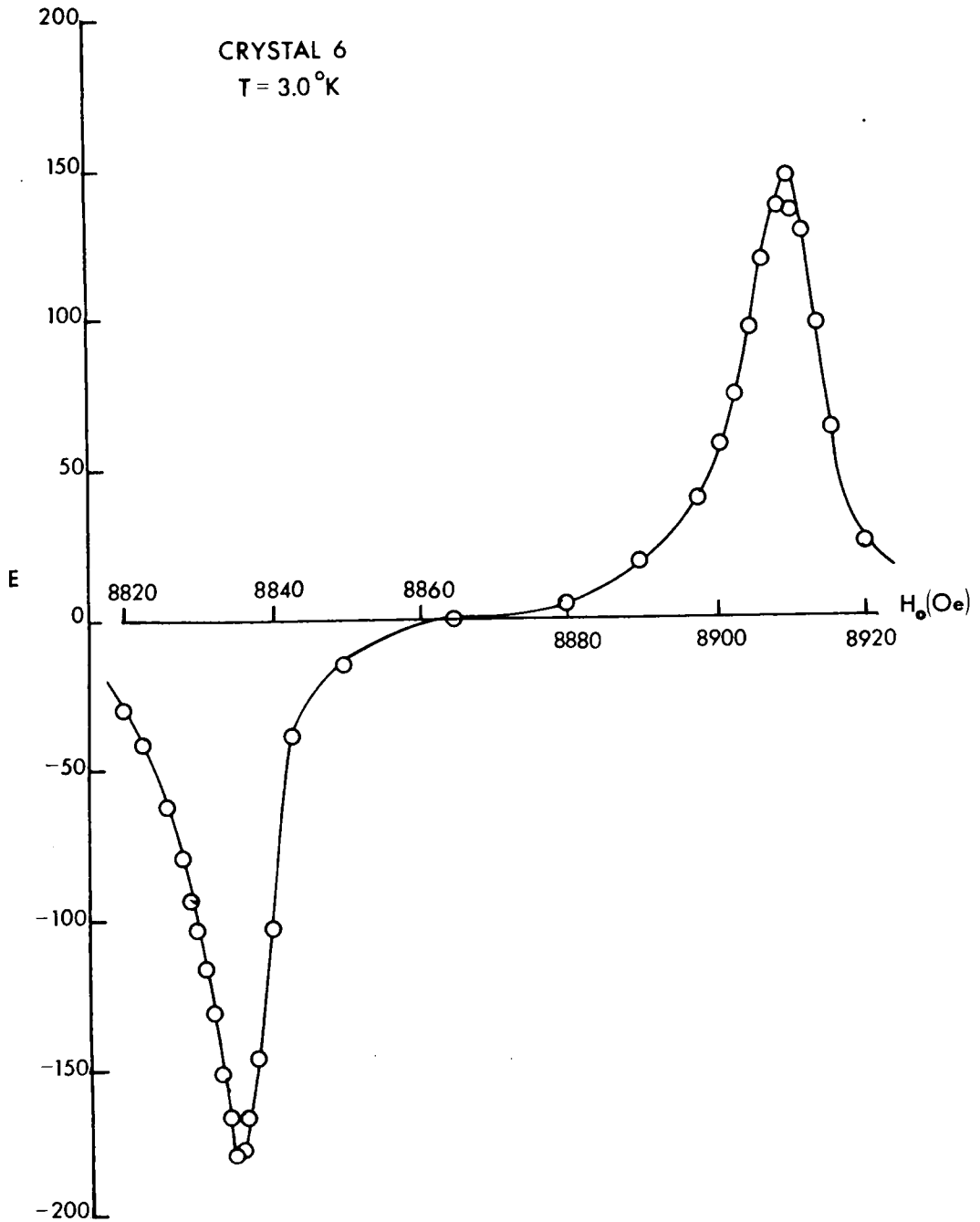


Figure 9.- Enhancement curve for crystal 6 at 3.0°K .

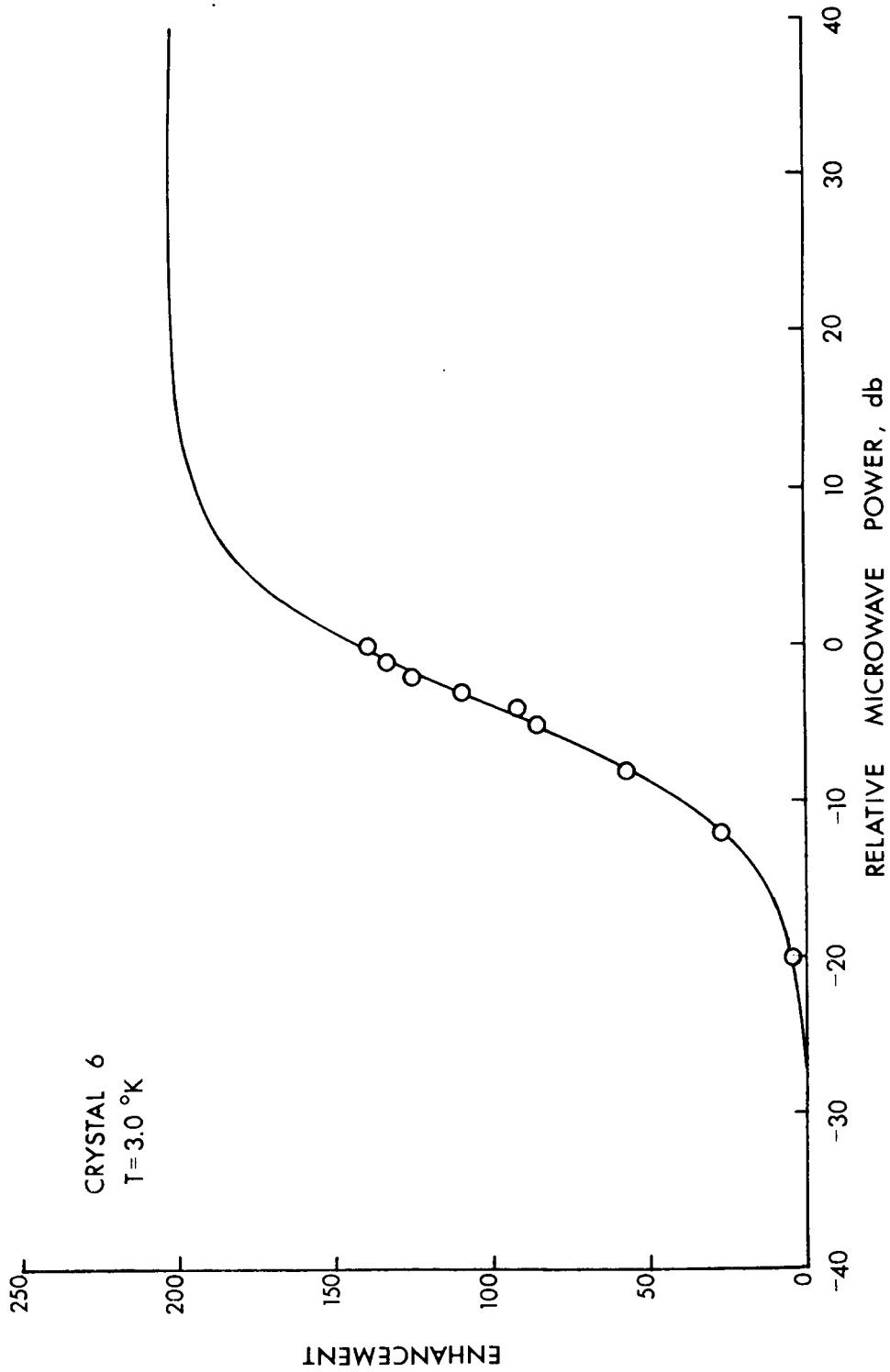


Figure 10.- Enhancement of the polarization peak as a function of relative microwave power for crystal 6.

The values of E' and S_0 determined by the computer fit are given as items 15 and 16, respectively, in table I. The curves drawn in figures 8 and 10 are equation (102) using the E' and S_0 values thus determined.

The experimental peak enhancements can be compared to the ideal enhancement, E_{ideal} , which is the ratio of the electron and nuclear Larmour frequencies, that is,

$$E_{\text{ideal}} = \frac{\omega_e}{\omega_n}, \quad (104)$$

by correcting for the leakage factor (nT_e/NT_n). The result of this correction is given as item 17 in table I.

The nuclear spin-lattice relaxation time, T_n , was measured as a function of bath temperature between 1.6° K and 4.2° K at a constant magnetic field value of 8970 Oe using crystal 7. These data are shown in figure 11.

A theoretical enhancement curve can be drawn if a line shape function for the ESR absorption is assumed. Equation (98) can be written in the form

$$E = \frac{1 + E' \left(\frac{S}{S_0} \right) \frac{g(\Delta H)}{g(0)}}{1 + \left(\frac{S}{S_0} \right) \frac{g(\Delta H)}{g(0)}} \quad (105)$$

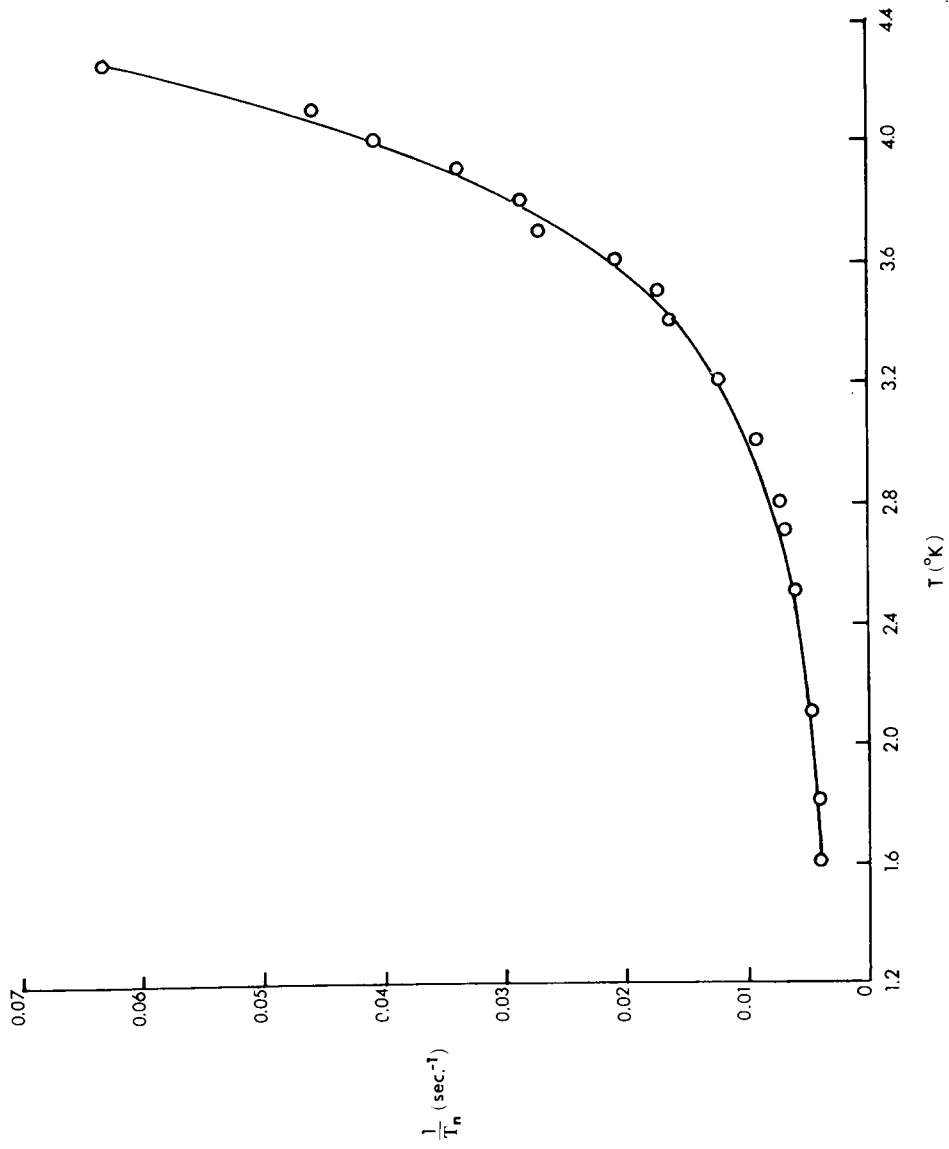


Figure 11.- The inverse of the nuclear spin lattice relaxation time of crystal 7 versus bath temperature for $H = 8970$ Oe.

using the terms defined in equations (102) and (103). We use here the shorthand notation $g(\Delta H)$ for $g(\omega_n \pm \Delta)$ which appeared in equation (67). Equation (102) was written for the peak enhancement at $g(0)$. The curve in figure 12 is equation (105) plotted for crystal 4 with maximum microwave power ($S = 1$ in our units), assuming a Gaussian line-shape function²⁶

$$\frac{g(\Delta H)}{g(0)} = e^{-2(\Delta H)^2 / (\Delta H_{pp}^e)^2} \quad (106)$$

with parameters from table I for crystal 4. The circles are the measured DNP enhancements.

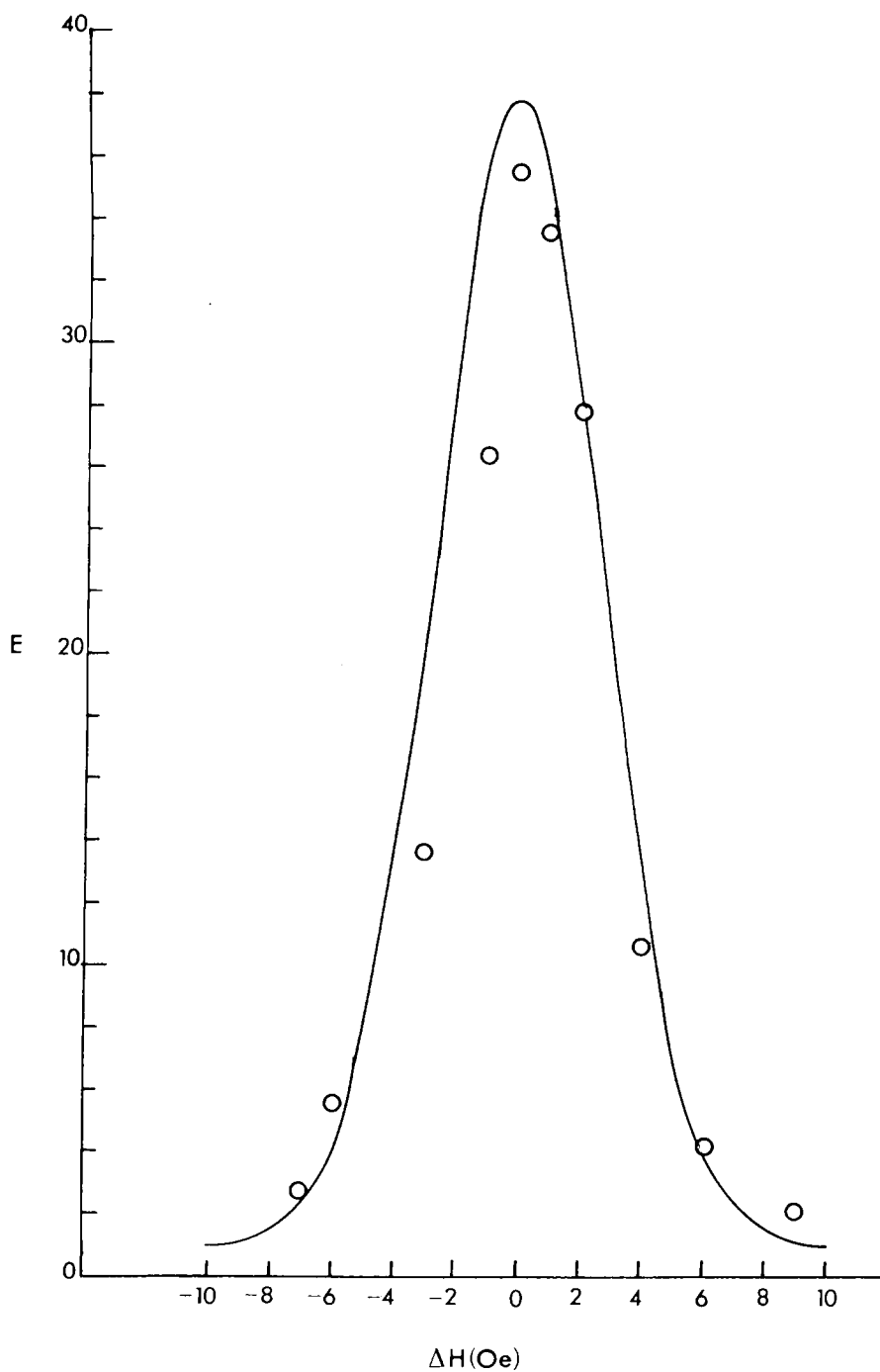


Figure 12.- Theoretical enhancement curve assuming a Gaussian line shape for the ESR and the experimental data for crystal 4.

V. DISCUSSION OF RESULTS AND CONCLUSIONS

The major objectives of this research were to derive the equations governing the dynamic nuclear polarization by the solid effect using the spin temperature theory (eqs. (80)) and to test this theory in the limit of well-resolved solid effect transitions. Single crystals of samarium doped lanthanum magnesium nitrate were used since the solid effect transitions of the samarium ion in the host lattice of lanthanum magnesium nitrate are well resolved from the main ESR transition.

The theory predicts a maximum, "ideal" enhancement E_{ideal} given in equation (104) for complete saturation at the center of the solid effect transition with negligible leakage. For the situations realized in this thesis

$$E_{\text{ideal}} = 240.$$

Data of the peak enhancement as a function of relative microwave power were obtained for crystals 2 through 7. In each case, the data indicated that insufficient power was available to completely saturate the solid effect transition (see, for example, figs. 8 and 10). The maximum enhancement can be predicted from this data if it is assumed that the enhancement as a function of power is given by equation (98), which was rewritten as equation (102). The extrapolated value of infinite microwave power enhancement (E' in eq. (102)) is given as item 15 in table I. Saturation was almost complete at 1.81° K for crystal 3 since the observed peak enhancement was 22 and the value E'

was 23.8. After the leakage factor was taken into account, the extrapolated maximum enhancement (item 17 in table I) was 245. This value is well within experimental error (± 20 percent) of the theoretical value, 240. The extrapolated maximum enhancements of crystals 4 and 6 were 20 percent lower than E_{ideal} even when corrected for leakage, which is the lower limit of our experimental error. The remaining crystals were not analyzed as above, or showed low enhancements. The reasons for the latter are not understood.

The theory predicts that for well-resolved solid effect transitions the enhancement extremums should be symmetrically situated about the main ESR transition and at

$$\omega = \omega_e \pm \omega_n .$$

Since it was difficult to establish the position of the center of the main ESR transition with respect to the positions of the peak enhancements, the solid effect separation (labeled as satellite separation, item 10 of table I) was used. This separation in oersteds should be

$$2H_0 \frac{\omega_n}{\omega_e} .$$

This value was calculated and is shown in table I. The measured separation is in excellent agreement with the calculated separation for each crystal and is well within the 5 Oe variation due to backlash in the incremental field controller.

The theory also predicts that for saturation conditions the absolute value of the enhancement extremums should be the same, that is,

$$E_{\max}^+ = E_{\max}^- .$$

A comparison of items 11 and 12 in table I indicates that this is true for most of the crystals and temperatures. However, in the values for crystal 6 at 3.0° K and crystal 7 at the two lower temperatures, E_{\max}^+ is up to 22 percent less than E_{\max}^- . This behavior has been observed before⁹ and was attributed to random drifting in the microwave apparatus.

The theoretical expression for the steady-state enhancement curve is a function of the ESR line-shape and microwave power. If these are known, a curve can be drawn predicting not only the positions of the enhancement extremums but also the shape of the enhancement curve. However, the ESR line-shape function was not computed from the measured ESR derivative curve in this experiment. Instead, a theoretical enhancement curve was drawn assuming a Gaussian line-shape²⁶ for the ESR line and using the values of E' and S_0 determined from the enhancement versus microwave power data for crystal 4; this is shown in figure 12 along with the experimental enhancement data for this crystal. The enhancement curve determined in this way is very sensitive to the derivative peak-to-peak width of the main ESR line.

The enhancement curves drawn through the experimental data in figures 7 and 9 do not agree with the theory in the region between the enhancement extremums. At approximately 10 Oe on either side of the enhancement extremums, the value of the enhancement should be +1. This deviation is attributed to the distorted line-shape of these crystals.

The theory of spin diffusion was incorporated into the spin temperature theory of the solid effect in order to account for the nuclear spin-lattice relaxation time. Only the case of rapid spin diffusion was considered, with the result that the nuclear spin-lattice relaxation rate should be given by equation (97), as can be seen from the analysis in section II F and the data in table II. If we assume that there is no leakage relaxation ($T_{n\lambda} \approx \infty$) and since the first term on the right side of equation (97) is negligible compared to the last term, then for crystal 7 we find

$$T_n = \frac{1}{W_1} + \frac{n}{N} \frac{\omega_n^2}{\omega_L^2} \frac{T_e}{2},$$

where we have used the relation¹⁴ $2T_D = T_e$. The nuclear spin-lattice relaxation time calculated from this equation results in times of the order of 10^2 seconds at 4.2° K and 10^5 seconds at 1.6° K. These calculated relaxation times differ from the experimentally determined relaxation times by one order of magnitude at 4.2° K and three orders of magnitude at 1.6° K. This deviation may be due to other paramagnetic impurities in the crystal that would result in a non-negligible leakage relaxation time. This mechanism would result in a measured relaxation time shorter than the theory would predict. Insufficient work was done to understand this discrepancy.

In conclusion, the equations governing the dynamic nuclear polarization by the solid effect using the spin temperature theory have been derived. For well-resolved solid effect transitions at microwave frequencies $\omega \approx \omega_e \pm \omega_n$, the expression for the steady-state

TABLE II.- NUCLEAR RELAXATION AND SPIN DIFFUSION PARAMETERS

FOR Sm:LMN

1. Samarium dilution (%) ^a	0.1	1.1
2. R (nm)	5.2	2.4
3. n/N	24,000	2,200
4. T _e (sec) ^b	2.5 × 10 ⁻⁵ - 0.10	2.5 × 10 ⁻⁵ - 0.10
5. T _{2e} (sec) ^c	3.6 × 10 ⁻⁸	3.6 × 10 ⁻⁸
6. T _{2n} (sec)	4.3 × 10 ⁻⁶	4.3 × 10 ⁻⁶
7. D (nm ² /sec)	930	930
8. C (nm ⁶ /sec) ^d	7.2 × 10 ⁻³ - 1.8 × 10 ⁻⁶	7.2 × 10 ⁻³ - 1.8 × 10 ⁻⁶
9. a (nm)	0.2	0.2
10. b (nm)	3.6 × 10 ⁻² - 4.5 × 10 ⁻³	3.6 × 10 ⁻² - 4.5 × 10 ⁻³
11. b ₀ (nm)	1.2	1.2
12. W ₁ (sec ⁻¹)	2.0 × 10 ⁻²	2.2 × 10 ⁻¹
13. $\frac{n\omega_n^2}{N\omega_L^2} W_1$ (sec ⁻¹)	3.1 × 10 ⁵	3.1 × 10 ⁵
14. $\left(\frac{1}{T_n}\right)$ (sec ⁻¹) ^e	2.9 × 10 ⁻⁵ - 7.2 × 10 ⁻⁹	3.2 × 10 ⁻⁴ - 7.9 × 10 ⁻⁸

^aX-ray fluorescence.

^bFrom reference 39.

^cEstimated from ESR peak-to-peak linewidth assuming that ESR line is completely homogeneously broadened.

^dFor $\omega_n T_e \gg 1$.

^eEstimated from equation (91).

enhancement differs from the expression obtained by the rate equation approach by small terms which become zero at $\omega = \omega_e \pm \omega_n$. The maximum enhancements extrapolated with the theory from those obtained experimentally agree with the ideal enhancement within experimental error for three of the crystals. The calculated satellite separation was within 6 percent of the measured separation for each of the enhancement curves, and the peak positive and negative enhancements were equal for all but two of the crystals. These results indicate that the spin temperature theory is a quantitatively correct approach for the description of dynamic nuclear polarization by the solid effect for well-resolved solid effect transitions.

VI. BIBLIOGRAPHY

1. A. Overhauser, Phys. Rev. 89, 689 (1953).
2. A. Overhauser, Phys. Rev. 92, 411 (1953).
3. F. Bloch, Phys. Rev. 93, 944 (1954).
4. A. Overhauser, Phys. Rev. 94, 768 (1954).
5. J. Korringa, Phys. Rev. 94, 1388 (1954).
6. A. Abragam, Phys. Rev. 98, 1729 (1955).
7. T. R. Carver and C. P. Slichter, Phys. Rev. 102, 975 (1956).
8. C. D. Jeffries, Dynamic Nuclear Orientation, (Interscience, New York, 1963).
9. T. J. Schmutge and C. D. Jeffries, Phys. Rev. 138, A1785 (1965).
10. O. S. Leifson and C. D. Jeffries, Phys. Rev. 122, 1781 (1961).
11. C. D. Jeffries, Technical Report No. UCB-34P20-T-1, Physics Department, University of California, 1966 (unpublished).
12. M. Borghini, Phys. Rev. Letters 16, 318 (1966).
13. M. A. Kozhushner and B. N. Provotorov, Fiz. Tver. Tela 6, 1472 (1964) [English transl.: Sov. Phys. -- Solid State 6, 1152 (1964)].
14. A. Abragam and M. Borghini, in Progress in Low Temperature Physics, edited by C. J. Gorter (North-Holland, Amsterdam, 1964), Vol. IV, Chap. VIII.
15. T. J. B. Swannenburg, G. M. Van den Heuvel, and N. J. Poulis, Physica 33, 707 (1967).
16. M. Goldman, Spin Temperature and Nuclear Magnetic Resonance in Solids, (Oxford University Press, London, 1970).
17. J. P. Boucher and M. Nechtschein, J. Phys. (Paris) 31, 783 (1970).
18. P. L. Scott, H. J. Stapleton, and C. Wainstein, Phys. Rev. 137, A71 (1965).
19. W. Low, Paramagnetic Resonance in Solids, (Academic Press, Inc., New York, 1960).

20. A. M. Portis, Phys. Rev. 91, 1071 (1953).
21. A. Messiah, Quantum Mechanics, (North-Holland, Amsterdam, 1964), Vols. I and II.
22. A. G. Redfield, Phys. Rev. 98, 1787 (1955).
23. D. S. Wollan, Rev. Sci. Instr. 42, 682 (1971).
24. B. N. Provotorov, Zh. Eksperim. i Teor. Fiz 41, 1582 (1961)
[English transl.: Sov. Phys. -- JETP 14, 1126 (1962)].
25. G. M. Van den Heuvel, C. T. C. Heyning, T. J. B. Swanenburg, and N. J. Poulis, Phys. Letter 27A, 38 (1968).
26. A. Abragam, The Principles of Nuclear Magnetism, (Oxford University Press, London, 1961).
27. N. Bloembergen, Physica 15, 386 (1949).
28. G. R. Khutsishvili, Usp. Fiz. Nauk 87, 211 (1965) [English transl.: Sov. Phys. -- Usp. 8, 743 (1966)].
29. G. R. Khutsishvili, Usp. Fiz. Nauk 96, 441 (1968) [English transl.: Sov. Phys. -- Usp. 11, 802 (1969)].
30. W. E. Blumberg, Phys. Rev. 119, 79 (1960).
31. P. G. de Gennes, J. Phys. Chem. Solids 7, 345 (1958).
32. D. S. Wollan, Thesis, University of Illinois, Urbana, 1966 (unpublished).
33. J. E. Berry and A. Benton, Rev. Sci. Instr. 36, 958 (1965).
34. J. P. Gordon, Rev. Sci. Instr. 32, 658 (1961).
35. F. G. Brickwedde, H. van Dijk, M. Durieux, J. R. Clement, and J. K. Logan, J. Res. Natl. Bur. Std. (U.S.) 64A, 1 (1960).
36. A. Zalkin, J. D. Forrester and D. H. Templeton, J. Chem. Phys. 39, 2881 (1963).
37. K. D. Bowers and J. Owens, Repts. Prog. Phys. 18, 304 (1955).
38. P. L. Scott and C. D. Jeffries, Phys. Rev. 127, 32 (1962).
39. G. H. Larson and C. D. Jeffries, Phys. Rev. 141, 461 (1966).
40. G. H. Larson and C. D. Jeffries, Phys. Rev. 145, 311 (1966).

VII. APPENDIX

A. Complete Expression of the Steady-State Enhancement

The complete expression for the enhancement of the nuclear polarization can be obtained from equations (80) by setting all the time derivatives equal to zero and solving for β using Cramer's Rule.

The result is

$$E = \frac{\beta}{\beta_L} = \frac{P}{Q}$$

where

$$\begin{aligned} P = & 1 + W^- \bar{T}_n \left(\frac{\omega_e}{\omega_n} + \frac{\omega_n - \Delta}{\omega_n} + \frac{n}{N} \frac{T_e}{\bar{T}_n} + \frac{n}{N} \frac{(\omega_n - \Delta)^2}{\omega_L^2} \frac{T_D}{\bar{T}_n} \right) \\ & + W^+ \bar{T}_n \left(-\frac{\omega_e}{\omega_n} + \frac{\omega_n + \Delta}{\omega_n} + \frac{n}{N} \frac{T_e}{\bar{T}_n} + \frac{n}{N} \frac{(\omega_n + \Delta)^2}{\omega_L^2} \frac{T_D}{\bar{T}_n} \right) \\ & + W^0 T_e \left(1 + \frac{\Delta^2}{\omega_L^2} \frac{T_D}{T_e} \right) + W_1 \bar{T}_n \left(1 + \frac{n}{N} \frac{\omega_n^2}{\omega_L^2} \frac{T_D}{\bar{T}_n} \right) \\ & + W^0 T_e (W_1 \bar{T}_n + W^+ \bar{T}_n + W^- \bar{T}_n) \left(1 + \frac{\Delta \omega_e}{\omega_L^2} \frac{T_D}{T_e} + \frac{n}{N} \frac{\omega_n^2}{\omega_L^2} \frac{T_D}{\bar{T}_n} \right) \end{aligned}$$

and

$$\begin{aligned}
Q = & 1 + W_{\bar{T}_n}^- \left(1 + \frac{n}{N} \frac{T_e}{\bar{T}_n} + \frac{n}{N} \frac{(\omega_n - \Delta)^2}{\omega_L^2} \frac{T_D}{\bar{T}_n} \right) \\
& + W_{\bar{T}_n}^+ \left(1 + \frac{n}{N} \frac{T_e}{\bar{T}_n} + \frac{n}{N} \frac{(\omega_n + \Delta)^2}{\omega_L^2} \frac{T_D}{\bar{T}_n} \right) \\
& + W_1 \bar{T}_n \left(1 + \frac{n}{N} \frac{\omega_n^2}{\omega_L^2} \frac{T_D}{\bar{T}_n} \right) \\
& + W_0 T_e \left[\left(1 + \frac{\Delta^2}{\omega_L^2} \frac{T_D}{T_e} \right) (1 + W_1 \bar{T}_n + W_{\bar{T}_n}^+ + W_{\bar{T}_n}^-) \right. \\
& \left. + \frac{n}{N} \frac{\omega_n^2}{\omega_L^2} (W_1 T_D + W_{T_D}^+ + W_{T_D}^-) \right]
\end{aligned}$$

**The vita has been removed from
the scanned document**

DYNAMIC NUCLEAR POLARIZATION
IN SAMARIUM DOPED LANTHANUM MAGNESIUM NITRATE

by

Charles E. Byvik

ABSTRACT

The dynamic nuclear polarization of hydrogen nuclei by the solid effect in single crystals of samarium doped lanthanum magnesium nitrate (Sm:LMN) has been studied theoretically and experimentally. The equations of evolution governing the dynamic nuclear polarization by the solid effect have been derived in detail using the spin temperature theory and the complete expression for the steady-state enhancement of the nuclear polarization has been calculated. For well-resolved solid effect transitions at microwave frequencies $\omega \approx \omega_e \pm \omega_n$, the expression for the steady-state enhancement differs from the expression obtained by the rate equation approach by small terms which become zero at $\omega = \omega_e \pm \omega_n$. Experimental enhancements of the proton polarization were obtained for eight crystals at 9.2 GHz and liquid helium temperatures. The samarium concentration ranged from 0.1 percent to 1.1 percent as determined by X-ray fluorescence. A peak enhancement of 181 was measured for a 1.1 percent Sm:LMN crystal at 3.0° K. The maximum enhancements extrapolated with the theory using the experimental data for peak enhancement versus microwave power and correcting for leakage, agree with the ideal enhancement (240 in this experiment) within experimental error for three of the crystals. The calculated satellite

separation was within 6 percent of the measured separation for each of the enhancement curves and the peak positive and negative enhancements were equal for all but two of the crystals. The nuclear spin-lattice relaxation time was measured for one of the crystals between 1.6° K and 4.2° K. To account for nuclear spin-lattice relaxation, spin diffusion theory in the rapid diffusion limit was incorporated into the results of the spin temperature theory of the solid effect. The experimental results indicate that the spin temperature theory is a quantitatively correct approach for the description of dynamic nuclear polarization by the solid effect for well-resolved solid effect transitions.